DIFFICULTIES IN PREDICTING THE RESPONSE OF A STRUCTURE FORMED BY COUPLING IDENTICAL SUBSTRUCTURES

BY
VISHWANATHA G. M.

DEPARTMENT OF MECHANICAL ENGINEERING
INDIAN INSTITUTE OF TECHNOLOGY, KANPUR
September 1989

DIFFICULTIES IN PREDICTING THE RESPONSE OF A STRUCTURE FORMED BY COUPLING IDENTICAL SUBSTRUCTURES

A Thesis Submitted
In Partial Fulfilment of the Requirements
for the degree of
MASTER OF TECHNOLOGY

BY
VISHWANATHA G. M.

to the
DEPARTMENT OF MECHANICAL ENGINEERING
INDIAN INSTITUTE OF TECHNOLOGY, KANPUR
September 1989

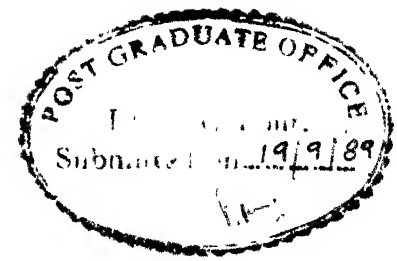

CERTIFICATE

This is to certify that the work entitled, "Difficult: in Predicting the Response of a Structure Formed by Coupling Identical Substructures" by Vishwanatha G.M. has been carrie out under my supervision and has not been submitted elsewher for a degree.

September, 1989.

(H. Hatwal)
Assistant Professor
Department of Mechanical Engineering
Indian Institute of Technology
Kanpur

ACKNOWLEDGEMENTS

I express my sincere gratitude to my guide Dr. H. Hatwal for his invaluable guidance and constant encouragement at all stages of work.

I thank Shastri for his constant guidance during my stay at I.I.T. Kanpur.

My thanks are due to Mr. M.M. Singh and Mr.Majumdar of Vibration Lab. for all the help extended to me.

I express my thanks to Ramesh, Ganesh, Shridhar, Anil Kumar, Ganesan, Srivastava, Ravindra, Sanjay Varma and a host of other friends for making my stay at I.I.T. a most enjoyable and memorable one.

-Vishwanatha G.M.

CONTENTS

LIST OF FIGURES

GENERAL NOTATIONS

x_i, y_i	Translational coordinates at point i
x, a	Acceleration
$\bar{\theta}_i$	Response to torsional vibrations of beam i
$\bar{y}_i$	Response to bending vibrations of beam i
f_i	Force at point i
M	Moment
T	Torque
2Γ	Included angle between the two beam elements
l	Length of beam
a	Width of beam
b	Thickness of beam
ω, p	Frequency in rad/sec.
ω_r	Natural frequency (rth mode)
η_r	Hysteritic damping loss factor for rth mode
$[\emptyset]$	Matrix of mode shape vectors
$_rA_{jk}$	Modal constant (mode r, FRF α_{jk})
$\bar{a}$	Accelerance
α	Receptance
Z	Impedance
$\alpha^a_{y_1\theta_1}$	Receptance of component A (y_1 and θ_1 are coordinates).

ABSTRACT

The objective of the present work is to predict the vibrational behaviour of a coupled structure (formed by coupling two identical beam elements), when the response characteristics of each individual beam member is known from experimental modal testing. The beam elements are connected at their ends using a single bolt. This arrangement facilitates the two beams to be bolted together at any desired angle between the beams. The out-of-plane oscillations are considered so that when the longitudinal axes of the beam members are not collinear then the bending and torsional modes get coupled. Theoretical and experimental analysis is carried out. Theoretical analysis gives a good prediction of the natural frequencies of the coupled structure for various angles of coupling. Impedance coupling method is used in the experimental analysis. The substructure response data are obtained using single degree of freedom circle fit method. The coupling models considered account for the coupling of beams at various number of points with various degrees of freedom (translational and rotational). The experimental models have failed to yield a good prediction of the response of the coupled structure.

CHAPTER 1

INTRODUCTION

1.1 Introduction:

The dynamic testing is being extensively incorporated for the design development, quality control and qualification of products in industries. Experimental Modal Analysis is an important technique which is being widely used for this purpos Much development has taken place in the last two decades in this area of applied science. The primary objective is to determine or predict the dynamic behaviour of the test object. This information can then be used for fault diagnosis, design improvement and evaluation of operational capability of a syste Modal testing is also used to pinpoint and improve the modellir inaccuracies of finite element analysis.

An important application of experimental modal analysis is in the prediction of response of a coupled structure. The coupled structure is an assembly of substructures. If the response characteristics of these substructures in isolation is known, then the response of the coupled structure can be obtained using a coupling technique. The prediction of respons of a coupled structure from the responses of substructure offer the following advantage. The substructures can be modified in isolation and the combined effect of these modifications can be

studied quickly without having to perform the modal testing and analysis for the complete coupled structure. Some typical applications in the aircraft structures are listed below.

(i) Modification of mass, stiffness and damping properties of aircraft components. (ii) Modification of inertia properties in the usually large number of various wing-with-stores configuration of fighter aircrafts. (iii) Attachments of additional boosters to a launcher system. (iv) Payload alterations of space systems, for instance, by exchanging the entire payload module of a shuttle.

1.2 Literature Review:

This section restricts the literature review to coupled structure responses using modal testing. The literature concerning the development of Modal testing is covered in recent works by Jaspal Singh [1] and Vasudeva Rao [2].

Coupling techniques can be broadly classified into impedance coupling method and modal coupling method [3]. Modal testing combined with finite element models is employed widely for analysing the coupled structures [4].

In impedance coupling method, the measured frequency response data of substructures of a coupled structure are used to predict the response of the coupled structure. The number of degrees of freedom that are to be considered at each

coupling point is an important aspect. This depends upon the symmetry of structure and nature of the coupling. The coordinates associated with degrees of freedom can be classified as translational coordinates and the rotational coordinates. Measurement of oscillations along translational coordinates is straightforward and can be done, for example, with an accelerometer. The techniques available for the measurement of rotational coordinates and the techniques for providing moment and torque excitation are limited.

Smith [5] has developed a method for the application of couple. Twin shakers are used to apply either a direct force (with the two shakers in phase) or a couple (with them in ant phase). Ewins and Sainsbury [6] have outlined a method which uses a single shaker. A specially designed exciting block is attached to the test specimen at the coupling point. Forces are applied and measurements are made at different points and in different directions to obtain the mobility matrix which considers the rotational coordinates.

Sattinger [7] discussed a method in which rotational mobilities are derived as the spatial derivatives of the translational mobilities using finite difference technique. Chen and Cherng [8] have given a simple method for the measurement of rotational mobility. Rotational effects are approximated by reducing parallel force systems separated by a small distance to an equivalent force-couple systems.

The literature available in the area of coupling with modal test data is relatively small. Ewins and Sainsbury [6] have analysed the coupling of a beam with a block. Impedance coupling method was used. Two components were bolted together at a single point. Three degrees of freedom were considered at the coupling point. The results exhibited a good prediction.

An interesting problem of analysis of coupled helicopter carrier has been carried out by Ewins, Silva and Maleci [9]. Goyder [10] has discussed structural modelling from measured frequency response data. An error analysis of impedance couplir method is made. It is concluded that the response predicted fro impedance coupling method can only be best treated as a guide to the average response of the structure rather than as a detailed prediction.

Ewins [3] describes two modal coupling methods. The modal models of the substructures are used to determine the required substructure impedances. In method 1, the impedance coupling technique is recast in a form which directly gives the solution for modes of the coupled system. Method 2 (flexible coupling method) assumes the existence of a spring and/or dashpot element between each pair of connected subsystems. Both the methods finally reduce to a standard eigenvalue problem.

A discussion of different types of modal coupling namely Rigid, Flexible and Mixed coupling can be found in [11]. Conver gence problems due to frequency range truncation and incomplete load conditioning in the coupling points, statically determinate

and overdeterminate coupling conditions are also discussed.

Most of the work found in the literature employ a combined modal testing and finite element technique to analyse the coupled structures. A good review of literature of such a combined technique is given by Grief [4]. Chen and Cherng [8] have outlined a combined technique. Coupling of a beam with a beam and a beam with a plate was discussed. Lee [12] has used modal testing, condensation method (of FEM) and sensitivity analysis for dynamic modelling of structures with bolted and bearing joints. Condensation technique (static and dynamic condensation) is a numerical technique used for reducing the computation by reducing the order of the matrices [13].

Component Mode Synthesis is another reduction technique used in finite element modelling of the components. The basic principles involved in component mode synthesis is explained in [14]. Grief [4] has given a review of the literature in this area.

1.3 Objective and Scope of the Present Work:

This work was undertaken to investigate the coupling of two beam elements. Two beam elements bolted together by a single bolt form the coupled structure. This type of coupling facilitates the beams to be coupled at different included angles. The objective of the work is to examine the variation

in the vibrational behaviour of the coupled structure when the two beams are coupled at different angles. The objective was to develop both theoretical and experimental formulations. Both theoretical and experimental analysisare carried out under free-free conditions.

A closed form theoretical formulation is presented in Chapter 2. This formulation considers the coupling of out-of plane bending vibrations with the torsional vibrations of the coupled structure when the beams are coupled nonsymmetrically.

Impedance coupling technique is used to study the coupling experimentally. The number of points considered for coupling and the associated coordinates at each point are explained in Chapter 3.

In Chapter 4, the modal testing is used to obtain the modal parameters for the substructures and these are used to predict the response of the coupled structure. A comparison is also made therein to compare the predicted and experimentall measured responses. Chapter 5 presents a general discussion on the results obtained from various coupling models.

CHAPTER 2

THEORETICAL FORMULATION

2.1 Introduction:

This chapter deals with the theoretical formulation for the coupled bending and torsional vibrations of the coupled structure (section 2.2). In section 2.3, a comparison of theoretically obtained natural frequencies with the experimentally measured ones is given.

In the theoretical formulation, the coupled out-of plane bending and torsional vibrations is dealt with. The theory of bending vibrations is based on the Bernoulli-Euler beam theory. Literature dealing with the coupled out-of plane bending and torsional vibrations is not known. Chang [17] discussed the in-pl vibrations of frames and trusses with inclined members.

2.2 Formulation for Coupling of Out of Plane Bending and Torsional Modes of Free Beams

Consider two free-free beam elements of rectangular cross-section joined at their ends (Fig. 2.1). Figure 2.1 shows the global (X-Y - Z) coordinate system and the local (x_i - y_i - z_i) coordinate systems attached to the beams. The included angle between the two beams is denoted by 2Γ. Let $\bar{y}_i(t, x_i)$ and $\bar{\theta}_i(t, x_i)$ be the bending and torsional response

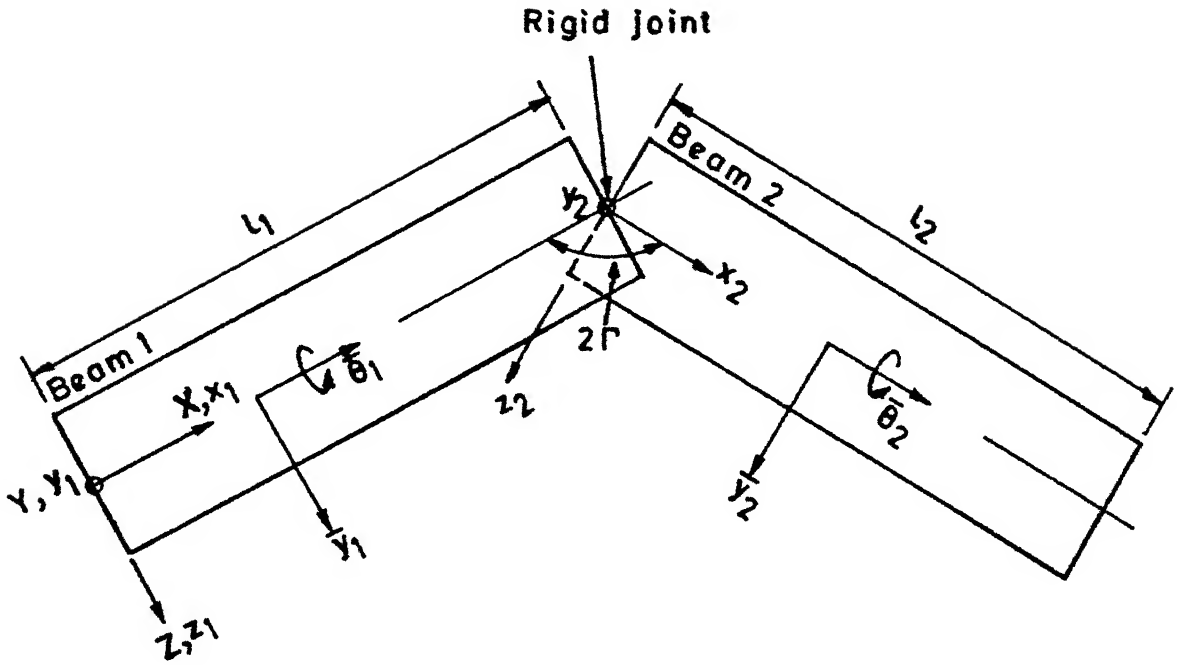

FIG. 2-1 COORDINATE SYSTEMS ON THE COUPLED STRUCTURE

coordinates. The equation of motion for $\bar{y}_i$ and $\bar{\theta}_i$ are,

$$\frac{d^2 \bar{y}_i}{dt^2} + \beta_{ib}^2 \frac{d^4 \bar{y}_i}{d x_i^4} = 0 \qquad 2.1(a)$$

and

$$\frac{d^2 \bar{\theta}_i}{dt^2} - \beta_{i\theta}^2 \frac{d^2 \bar{\theta}_i}{d x_i^2} = 0 . \qquad 2.1(b)$$

where,

$$\beta_{ib}^2 = \frac{E_i I_i}{\rho_i A_i} \; ; \; \beta_{i\theta}^2 = \frac{G_i C_i}{\rho_i I_{pi}}$$

and E_i is the modulus of elasticity, I_i is the area moment of inertia, A_i is the area of cross-section, ρ_i is mass density, G_i is shear modulus, C_i is torsional constant [16] and I_{pi} is the polar moment of inertia of the ith (i = 1,2) bar. (Geometric and material properties used in the present work are given in Appendix A).

To study the natural modes, the oscillations are assumed to be harmonic so that

$$\begin{aligned} \bar{y}_i (t,x_i) &= y_i(x_i)\mathrm{Sin}pt \\ \bar{\theta}_i (t,x_i) &= \theta_i(x_i)\mathrm{Sin}pt \qquad (i = 1,2) \end{aligned} \qquad (2.2)$$

Substitution of (2.2) in (2.1) yields the form of solution as

$$Y_1(x_1) = d_1 \mathrm{Sin} K_{1b} x_1 + d_2 \mathrm{Cos} K_{1b} x_1 + d_3 \mathrm{Sinh}\, K_{1b} x_1 + d_4 \mathrm{Cosh} K_{1b} x_1$$

$$Y_2(x_2) = d_5 \mathrm{Sin} K_{2b} x_2 + d_6 \mathrm{Cos} K_{2b} x_2 + d_7 \mathrm{Sinh} K_{2b} x_2 + d_8 \mathrm{Cosh} K_{2b} x_2 \quad . \tag{2.3}$$

$$\theta_1(x_1) = d_9 \mathrm{Sin}\, K_{1\theta}\, x_1 + d_{10}\, \mathrm{Cos}\, K_{1\theta}\, x_1$$

$$\theta_2(x_2) = d_{11}\, \mathrm{Sin}\, K_{2\theta}\, x_2 + d_{12}\, \mathrm{Cos}\, K_{2\theta}\, x_2 \quad . \tag{2.4}$$

in which,

$$K_{ib} = \mathrm{SQRT}\ \left(\frac{p}{\beta_{ib}} \right) \text{ and } K_{i\theta} = p/\beta_{i\theta} \qquad (i=1,2)$$

p is the frequency of vibration in radians/sec. The constants of integration, d_is are to be determined from the boundary conditions.

The bending moment and torsion at cross-section at distance x_i are,

$$M_i = E_i I_i \frac{d^2 y_i}{d x_i^2} \tag{2.5}$$

and

$$T_i = G_i C_i \frac{d\theta_i}{dx_i} \quad (i = 1,2) \tag{2.6}$$

Free-free coupled system shown in Fig. 2.1, has the following six natural boundary conditions,

$$\text{At } x_1 = 0 \quad : \quad \frac{d\theta_1}{dx_1} = 0$$

$$: \quad \frac{d^2 y_1}{d x_1^2} = 0$$

$$: \quad \frac{d^3 y_1}{d x_1^3} = 0$$

$$\text{At } x_2 = l_2 \quad : \quad \frac{d\theta_2}{dx_2} = 0$$

$$: \quad \frac{d^2 y_2}{dx_2^2} = 0$$

$$: \quad \frac{d^3 y_2}{dx_2^3} = 0 \qquad (2.7)$$

Following are the six compatibility conditions at the joint ($x_1 = l_1$ and $x_2 = 0$):

(i) Displacement of both the beams should be equal

$$y_1 = y_2 \qquad (2.8)$$

(ii) Shear force balance at the joint yields

$$E_1 I_1 \frac{d^3 y_1}{dx_1^3} = E_2 I_2 \frac{d^3 y_2}{dx_2^3} \qquad (2.9)$$

(iii) Rotation of beam 1 and beam 2 in X-direction (Global) should be equal (Fig. 2.2)

$$\theta_1(l_1) = \theta_2(o)\,\mathrm{Cos}\psi - \frac{dy_2(o)}{dx_2}\,\mathrm{Sin}\psi$$

or $$\theta_1(l_1) = -\theta_2(o)\,\mathrm{Cos}\,2\Gamma - \frac{dy_2(o)}{dx_2}\,\mathrm{Sin}2\Gamma \qquad (2.10)$$

(iv) Rotation of beam 1 and beam 2 in Z-direction (i.e. Global) should be equal (Figure 2.2)

$$\frac{d\,y_1(l_1)}{dx_1} = \theta_2(o)\,\mathrm{Sin}\psi + \frac{dy_2(o)}{dx_2}\,\mathrm{Cos}\psi$$

or $$\frac{dy_1(l_1)}{dx_1} = \theta_2(o)\,\mathrm{Sin}\,2\Gamma - \frac{dy_2(o)}{dx_2}\,\mathrm{Cos}2\Gamma \qquad (2.11)$$

(v) Moments in Z-direction on the beams should belance (Fig. 2.3).

$$M_1 = T_2\,\mathrm{Sin}\psi + M_2\,\mathrm{Cos}\psi$$

or $$E_1I_1\,\frac{d^2y_1(l_1)}{dx_1^2} = G_2C_2\,\frac{d\theta_2(o)}{dx_2}\,\mathrm{Sin}2\Gamma - E_2I_2\,\frac{d^2y_2(o)}{dx_2^2}\,\mathrm{Cos}2\Gamma \qquad (2.12)$$

(vi) Moments in X-direction on the beams should balance (Fig. 2.3).

$$T_1 = T_2\mathrm{Cos}\psi - M_2\,\mathrm{Sin}\psi$$

or $$G_1C_1\,\frac{d\theta_1(l_1)}{dx_1} = -G_2C_2\,\frac{d\theta_2(o)}{dx_2}\,\mathrm{Cos}2\Gamma - E_2I_2\,\frac{d^2y_2(o)}{dx_2^2}\,\mathrm{Sin}2\Gamma \qquad (2.13)$$

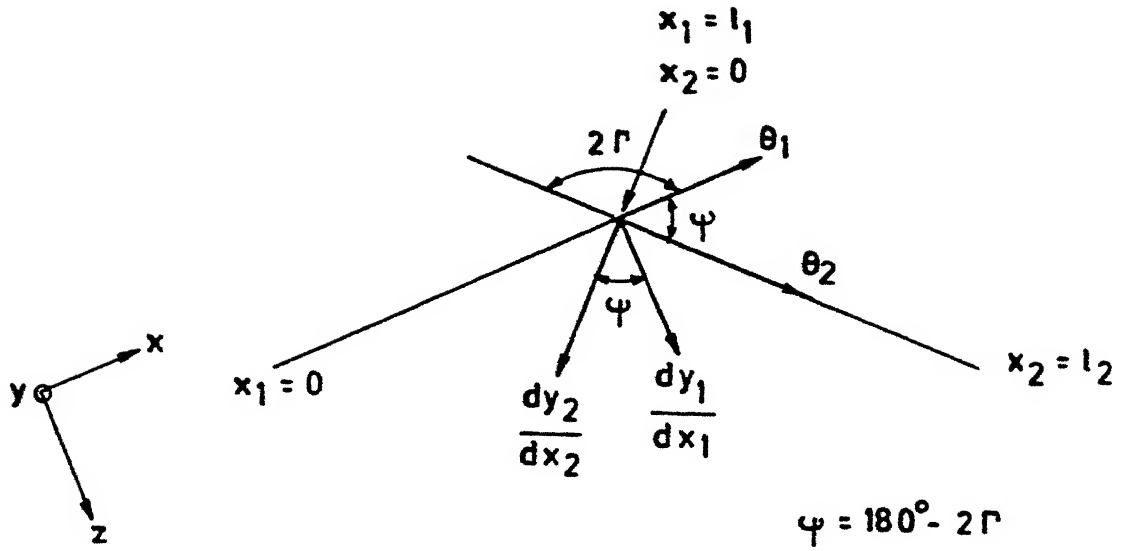

FIG. 2·2 RESOLUTION OF COORDINATES IN x AND z DIRECTION

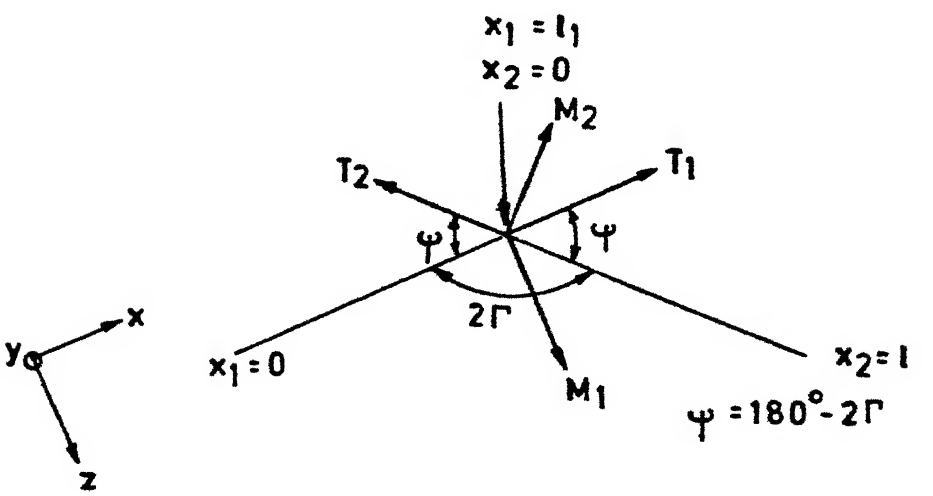

FIG. 2·3 RESOLUTION OF COUPLES IN x AND z DIRECTION

The first boundary condition of (2.7), i.e. $\theta_1'(o) = 0$, gives one of the constants of integration $d_9 = 0$. Substitution of (2.3) and (2.4) in (2.7) to (2.13) gives a set of homogeneous equations of the form

$$[M] \{d\} = \{0\} \qquad (2.14)$$

where

[M] is 11x 11 square matrix and {d} is column matrix of eleven constants, such that

$$\{d\} = \{d_1, d_2, d_3, d_4, d_5, d_6, d_7, d_8, d_{10}, d_{11}, d_{12}\}^T$$

and the elements of matrix [M] are given in Appendix F.

For non-trivial solution, the deteriment of matrix [M] should vanish. The parameters K_{ib} and $K_{i\theta}$ in the elements of matrix [M] contain the frequency, p. The value of p at which the determinant becomes zero is noted as the natural frequency of the system.

2.3 Verification of Theoretical Results:

Two beams, of dimensions and properties outlined in Appendix A were coupled at various values of the included angle. Equation (2.14) was used to determine the natural frequencies of the coupled structure. Numerical computation was carried out at the step of 1Hz.

An experimental verification for these results was also performed. Two beams of the same specifications were bolted. An impact hammer was used to excite coupled beam structure under free-free condition.

Table 2.1 gives a comparison between natural frequencies obtained theoretically and experimentally for two values of included angle (2Γ). The torsional and bending modes for $2\Gamma = 180^{\circ}$ are identified in Table 2.1 since these modes are uncoupled. For other values of included angle it will be more meaningful to talk in terms of symmetric and unsymmetric modes. Included angle being zero is a special case. Fig. 2.4 presents the results for $\Gamma = 0$ but these results are not clubbed with the other results obtained for different values of 2Γ, because the phys. interpretation can not be attempted without looking at the modes. Fig. 2.5(a) and (b) give two experimentally measured frequency response functions of the coupled structure for $2\Gamma = 90^{\circ}$ and $2\Gamma = 180^{\circ}$ respectively.

In the experiment, the two beams overlap on each other reducing the effective length of the coupled structure (in case of $2\Gamma = 180^{\circ}$). But in the theoretical formulation the beams couple at one point making the length of the coupled structure (in case of $2\Gamma = 180^{\circ}$) equal to the sum of the lengths of individual elements. Moreover, the nature of coupling between bending and torsional modes is strongly dependent on the included angle. Therefore, it cannot be said conclusively that the natural frequencies, as obtained from experiment, will always be higher

Table 2.1 Theoretically and Experimentally Measured Values of Natural Frequencies for 2Γ = 90 and 2Γ = 180°

Included angle (2Γ)	Theoretically obtained natural frequencies (upto 2000 Hz)	Experimentally measu natural frequencie (upto 2000 Hz)
90°	236	272
	310	304
	532	608
	544	624
	848	964
	1032	1004
	1537	1612
	1563	1624
	1879	--
180°	89 (bending mode)	100
	246 (bending mode)	288
	481 (bending mode)	528
	615 (torsional mode)	704
	795 (bending mode)	908
	1187 (bending mode)	1196
	1230 (torsional mode)	1316
	1657 (bending mode)	1808
	1845 (torsional mode)	--

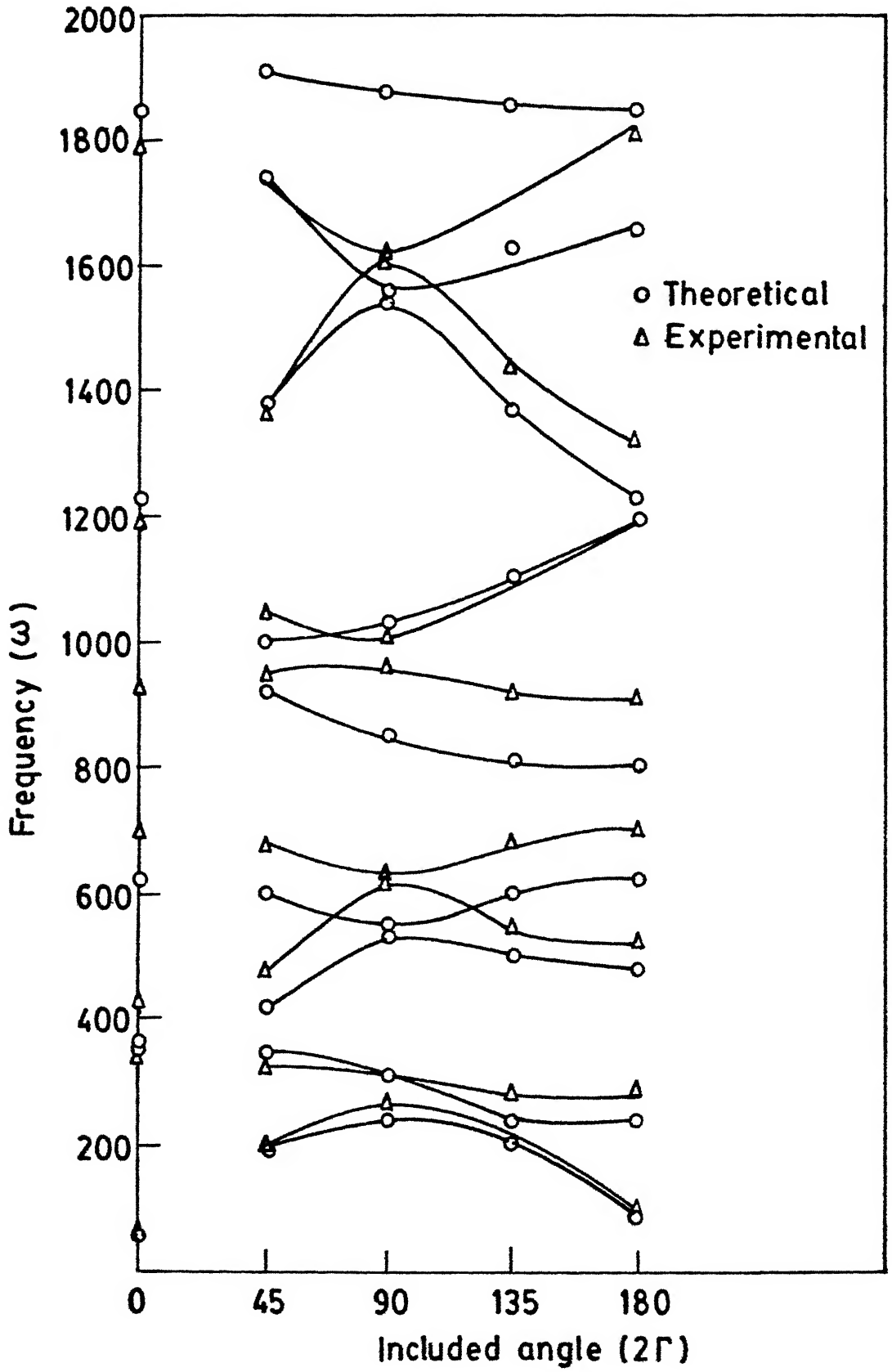

FIG. 2.4 COMPARISON OF THEORETICAL AND EXPERIMENTAL NATURAL FREQUENCIES

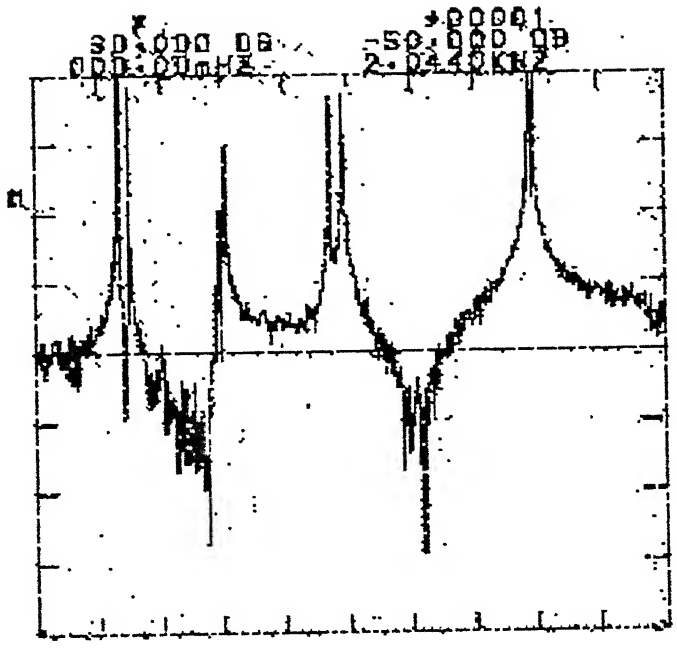

At $2\Gamma = 90^{\circ}$

Fig. 2.5(a)

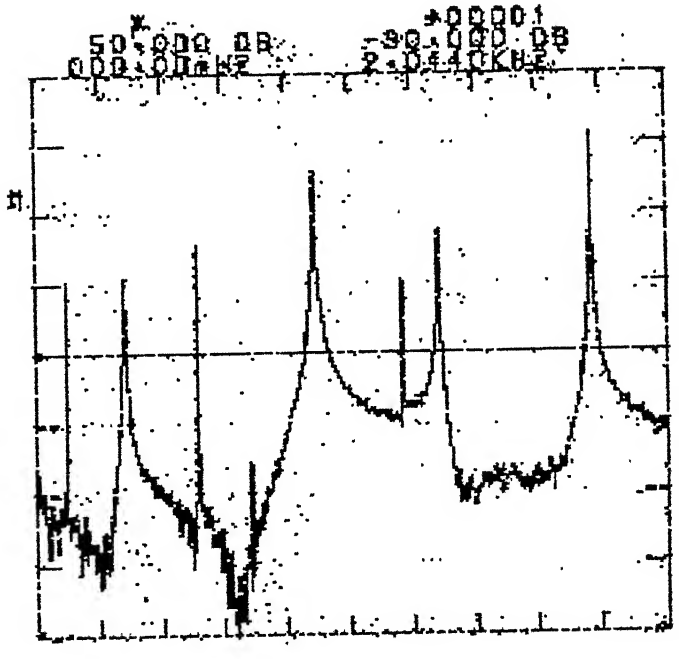

At $2\Gamma = 90^{\circ}$

Fig. 2.5(b)

Fig 2.5 : FRF of coupled structure for two values of 2Γ

than the theoretical ones. But generally the experimental values are on the higher side.

CHAPTER 3

THEORY OF IMPEDANCE COUPLING USING EXPERIMENTAL FRFs

3.1 Introduction:

This chapter explains briefly the theory of impedance coupling methods. Different types of Frequency Response Functions (FRFs) and the relevant definitions are detailed in Appendix B. First a method is outlined for the coupling of two substructures at a single coordinate. Then the procedure is outlined for coupling at more than one coordinate with more than one degree of freedom. Inclusion of the coordinates in the analysis which are not involved in the coupling is also examined. Section 3.3 explains in detail the various coupling models used in the present work.

3.2 Impedance Coupling Method:

This method is also called as Dynamic Stiffness Method [3]. The underlying principle is given below.

Consider two components A and B (Fig. 3.1) which are coupled at a single coordinate to form the coupled structure C. The coupling coordinate is designated by x_1 and the coincident coupling points on substructures A and B are denoted by numeric 1.

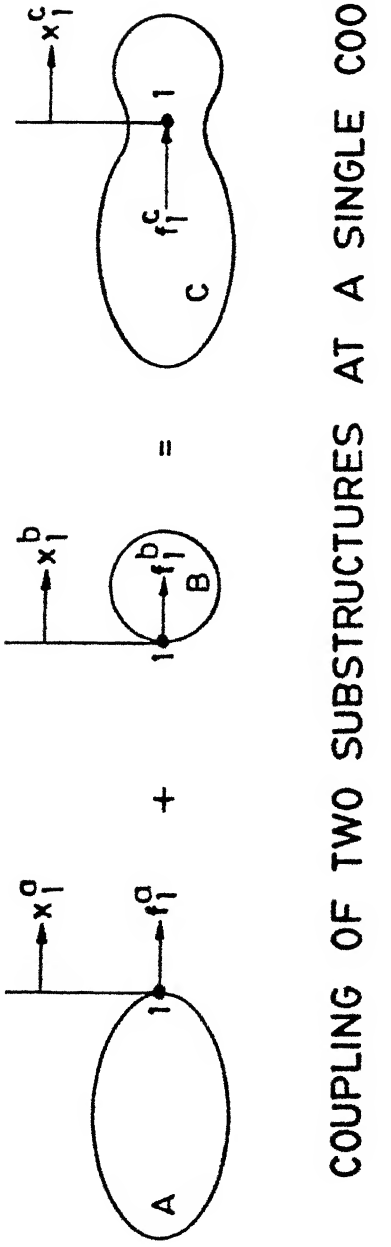

FIG. 3.1 COUPLING OF TWO SUBSTRUCTURES AT A SINGLE COORDINATE

The coupling point on the coupled structure 'C', is also denoted by 1.

If the system A at the connection point is excited harmonically by $f_1^a\, e^{i\omega t}$, the resulting response $x_1^a\, e^{i\omega t}$ is given by,

$$x_1^a\, e^{i\omega t} = \alpha^a_{x_1 x_1}(\omega)\ f_1^a\ e^{i\omega t} \tag{3.1}$$

or

$$x_1^a = \alpha^a_{x_1 x_1}(\omega)\ .\ f_1^a \tag{3.2}$$

Similarly for subsystem B,

$$x_1^b = \alpha^b_{x_1 x_1}(\omega)\ .\ f_1^b \tag{3.3}$$

Applying the compatibility and equilibrium conditions at the connection coordinates one gets,

$$x_1^a = x_1^b = x_1^c \tag{3.4}$$

$$f_1^c = f_1^a + f_1^b \tag{3.5}$$

Substitution of (3.2) and (3.3) in (3.5) and using the equation (3.4), the relationship between the receptances is

$$\frac{1}{\alpha^{c}_{x_1x_1}} = \frac{1}{\alpha^{a}_{x_1x_1}} + \frac{1}{\alpha^{b}_{x_1x_1}} \tag{3.6}$$

or

$$Z^{c}_{x_1x_1} = Z^{a}_{x_1x_1} + Z^{b}_{x_1x_1} \tag{3.7}$$

where Z denotes the impedance.

Thus the FRF of the coupled structure 'C' can be obtained in terms of the FRF properties of the substructures analysed separately.

The above analysis can be extended to the systems connected at more than one coordinate. At each coordinate more than one degree of freedom may be considered. The coordinates which are not involved in coupling may also be included. The whole process involves the partition of the subsystem impedance matrices into submatrices which are involved in coupling and those which are not. The submatrices involved in coupling are added to yield the resultant impedance matrix. Therefore, if $[\alpha^{a}(\omega)]$ and $[Z^{a}(\omega)]$ are the receptance and impedance matrices, respectively, of subsystems A and $[\alpha^{b}(\omega)]$ and $[Z^{b}(\omega)]$ are the corresponding matrices of subsystem B, and if the coupling coordinates are collectively designated by q, the coordinates not involved in coupling by p for subsystem A, then the receptance matrix is partitioned as

$$[\alpha^a(\omega)] = \begin{bmatrix} \alpha^a_{x_p x_p} & \alpha^a_{x_p x_q} \\ \alpha^a_{x_q x_p} & \alpha^a_{x_q x_q} \end{bmatrix} \tag{3.8}$$

$$[Z^a(\omega)] = [\alpha^a(\omega)]^{-1} = \begin{bmatrix} Z^a_{x_p x_p} & Z^a_{x_p x_q} \\ Z^a_{x_q x_p} & Z^a_{x_q x_q} \end{bmatrix} \tag{3.9}$$

Similarly, the impedence matrix for the subsystem B is given by,

$$[Z^b(\omega)] = [\alpha^b(\omega)]^{-1} = \begin{bmatrix} Z^b_{x_r x_r} & Z^b_{x_r x_q} \\ Z^b_{x_q x_r} & Z^b_{x_q x_q} \end{bmatrix} \tag{3.10}$$

where 'r' denotes the coordinates on the subsystem 'B' which are not involved in coupling.

The order of each submatrix in (3.9) and (3.10) depends upon the number of coordinates involved in the coupling and the number of degrees of freedom considered at each coordinate.

Now as before, applying the compatibility and equilibrium condition, one can obtain,

$$\frac{1}{[\alpha^c(\omega)]} = \frac{1}{[\alpha^a(\omega)]} \oplus \frac{1}{[\alpha^b(\omega)]} \tag{3.11}$$

where, $\oplus$ sign indicates the addition of partitioned matrices involved in coupling.

In other words, the impedence matrix $[Z_c(\omega)]$ for the coupled structure can be obtained in the form

$$[Z^c(\omega)] = [Z^a(\omega)] \oplus [Z^b(\omega)] \tag{3.12}$$

$$= \begin{bmatrix} Z^a_{x_p x_p} & 0 & Z^a_{x_p x_q} \\ 0 & Z^b_{x_r x_r} & Z^b_{x_r x_q} \\ Z^a_{x_q x_p} & Z^b_{x_q x_r} & Z^a_{x_q x_q} + Z^b_{x_q x_q} \end{bmatrix} \tag{3.13}$$

The receptance matrix $[\alpha^c(\omega)]$ for the coupled system is obtained by the inverse of $[Z^c(\omega)]$ as

$$[\alpha^c(\omega)] = [Z^c(\omega)]^{-1} \tag{3.14}$$

From modal testing point of view, the receptances required for the substructures may be evaluated by any one of the options mentioned below.

(1) Using the modal Model and evaluating the receptance matrix using the formula

$$[\alpha(\omega)] = [\emptyset] \left[(\lambda_r^2 - \omega^2) \right]^{-1} [\emptyset]^T \qquad (3.15)$$

where

$$\lambda_r^2 = \omega_r^2 (1 + i\eta_r)$$

(2) Calculating the receptance FRF matrix obtained by direct measurement.

(3) Calculating the regenerated receptance FRF matrix from the measured FRFs.

The results presented in Chapter 4 are by using the last method of utilising the regenerated FRFs.

3.3 Number of Points and Degrees of Freedom Considered for Coupling:

The equilibrium equations for coupling of substructures, which are undergoing bending oscillations, will require the conditions on shear forces and bending moments. Therefore, two degrees of freedom, namely, transverse displacement and angular rotation should be assigned to the coupling point. The simplified coupling analysis can start with coupling of only translational degree of freedom.

Figure 3.2, shows the type of coupling being considered in this work. The two beams are coupled with a bolt and nut. The simplest coupling model is assumed to couple the two beams at only two points. This is later increased to coupling at four points.

Thus the different combinations of number of points selected and the degrees of freedom assigned to each point is expected to yield differing predictions for the coupled structure The various models cosidered in the present work are presented in the following sections.

The notations used for the coordinates and points are as indicated in the corresponding figures. Initially the coupling is explained for an included angle of $2\Gamma = 180^{o}$.

3.3.1 One-point, One-dof Coupling:

Figure 3.3 shows the coupling points and the degree of freedom considered on each substructure A and B and also on the coupled structure 'C'. From eqn. (3.6), the receptance of coupled structure will be,

$$\frac{1}{\alpha^{c}_{y_1 y_1}} = \frac{1}{\alpha^{a}_{y_1 y_1}} + \frac{1}{\alpha^{b}_{y_1 y_1}}$$

If the substructure A and B are identical, then the substructure receptances $\alpha^{a}_{y_1 y_1}$ and $\alpha^{b}_{y_1 y_1}$ will also be similar. This will lead to the coupled structure receptance as

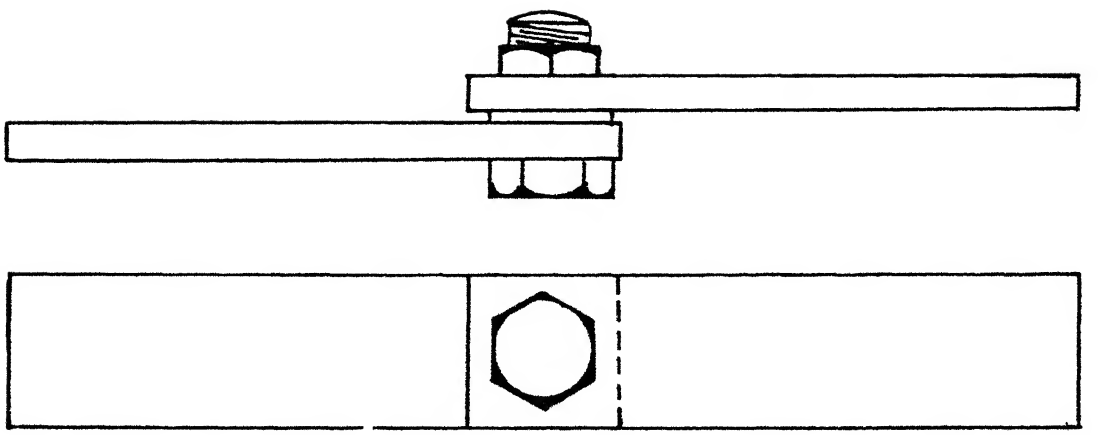

FIG. 3.2 COUPLED STRUCTURE

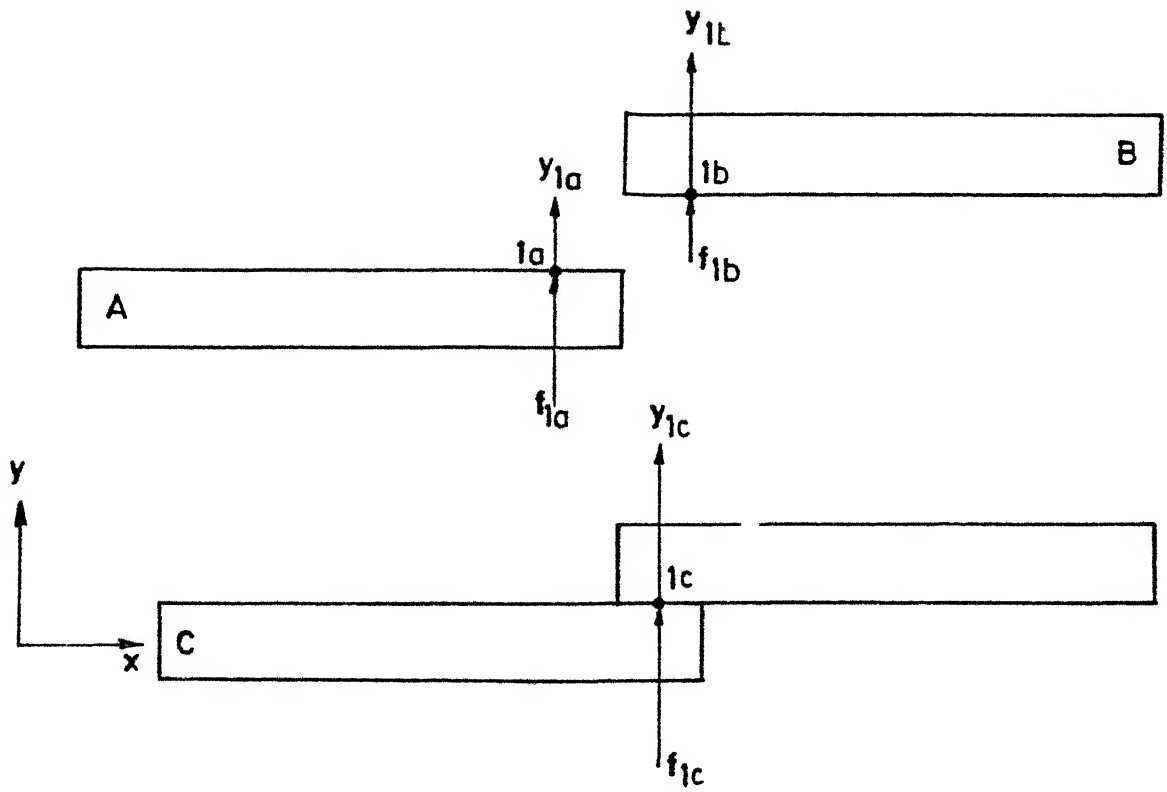

FIG. 3.3 ONE-POINT ONE- dof COUPLING MODEL

$$\frac{1}{\alpha^{c}_{y_1 y_1}} = \frac{1}{\alpha^{a}_{y_1 y_1}} + \frac{1}{\alpha^{b}_{y_1 y_1}}$$

where,

$$\alpha^{a}_{y_1 y_1} = \alpha^{b}_{y_1 y_1}$$

$$\alpha^{c}_{y_1 y_1} = \frac{1}{2}\alpha^{a}_{y_1 y_1}$$

or $$\alpha^{c}_{y_1 y_1} = \frac{1}{2}\alpha^{b}_{y_1 y_1}$$

which means that the coupled structure will have a similar FRF at the coupling point as its substructures. In fact the response of the coupling point on the coupled structure and the response of the corresponding point on the substructure will show peaks at same frequencies. For other natural frequencies of the coupled structure, this coupling point happens to be a node and hence $\alpha^{c}_{y_1 y_1}$ will not show any additional peaks. Obviously this model is applicable only to situations like longitudinal oscillations of free beams.

3.3.2 Two-point One-dof Coupling:

Figure 3.4 shows the coordinates and the degrees of freedom considered for the substructure and for the coupled structure.

From equation (3.11),

$$\frac{1}{[\alpha^c]_{y_2,y_3}} = \frac{1}{[\alpha^a]_{y_2,y_3}} \oplus \frac{1}{[\alpha^b]_{y_3,y_2}} \tag{3.16}$$

where,

$$[\alpha^a]_{y_2,y_3} = \begin{bmatrix} \alpha^a_{y_2y_2} & \alpha^a_{y_2y_3} \\ \alpha^a_{y_2y_3} & \alpha^a_{y_3y_3} \end{bmatrix} \quad \text{and} \quad [\alpha^b]_{y_3,y_2} = \begin{bmatrix} \alpha^b_{y_3y_3} & \alpha^b_{y_3y_2} \\ \alpha^b_{y_3y_2} & \alpha^b_{y_2y_2} \end{bmatrix}$$

where, Maxwell's reciprocity theorem has been used to make the receptance matrices as symmetric matrices. The impedance matrices are obtained as,

$$[Z^a]_{y_2y_3} = [\alpha^a]^{-1}_{y_2,y_3}$$

$$[Z^b]_{y_3y_2} = [\alpha^b]^{-1}_{y_3,y_2} \quad .$$

Now while coupling the substructures it can be noted from Figure 3.4, that the point 2a couples with the point 3b. This means that the impedance matrix of coupled structure will be,

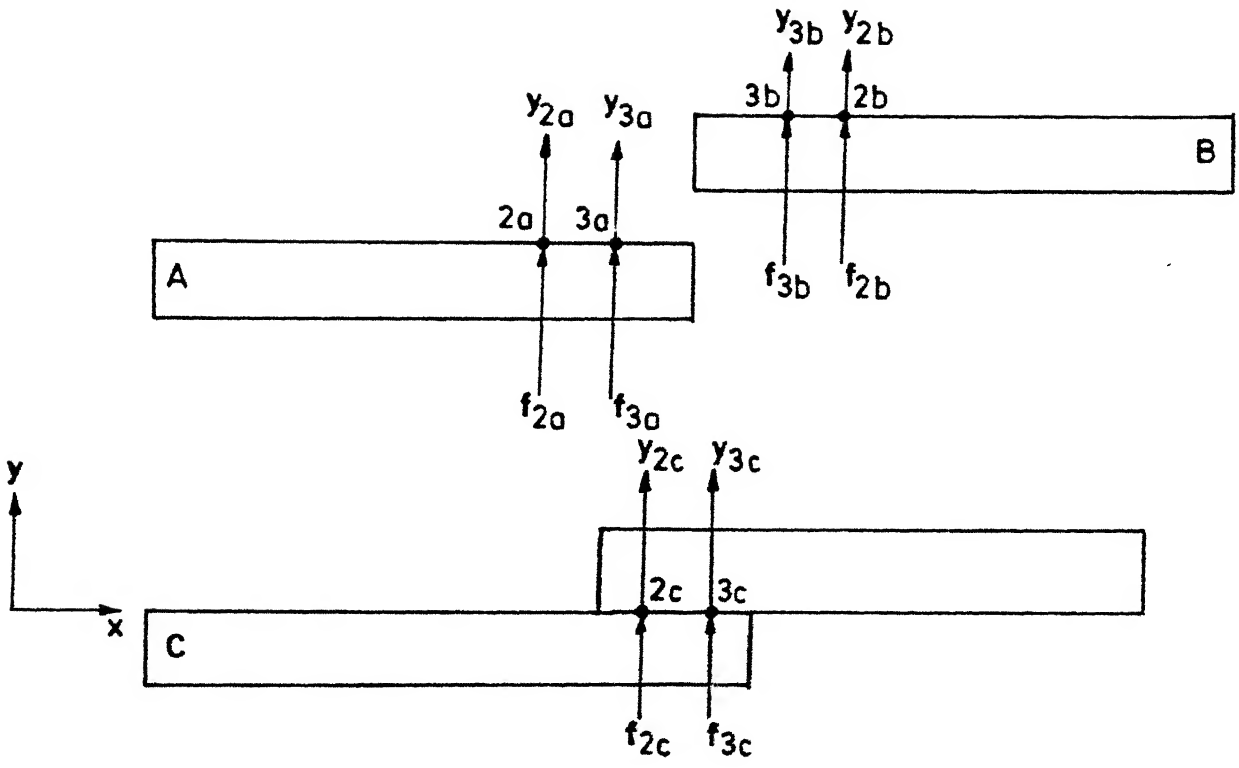

FIG. 3.4 TWO-POINT ONE-dof COUPLING MODEL

$$[z^c]_{y_2,y_3} = \begin{bmatrix} z^a_{y_2y_2} + z^b_{y_3y_3} & z^a_{y_2y_3} + z^b_{y_2y_3} \\ z^a_{y_2y_3} + z^b_{y_2y_3} & z^a_{y_3y_3} + z^b_{y_2y_2} \end{bmatrix} . \tag{3.17}$$

The two coordinates considered does not explicitly account for the effect of rotation due to bending but indirectly the effect of slope is introduced.

3.3.3 Four-point One-dof Coupling:

Figure 3.5, shows the coupling coordinates considered for the substructures and for the coupled structure. Proceeding in the manner explained in section 3.2, one can arrive at,

$$[z^a]_{y_3,y_5,y_2,y_6} = \begin{bmatrix} z^a_{y_3y_3} & z^a_{y_3y_5} & z^a_{y_3y_2} & z^a_{y_3y_6} \\ & z^a_{y_5y_5} & z^a_{y_5y_2} & z^a_{y_5y_6} \\ \text{Symmetric} & & z^a_{y_2y_2} & z^a_{y_2y_6} \\ & & & z^a_{y_6y_6} \end{bmatrix}$$

$$[z^b]_{y_2,y_6,y_3,y_5} = \begin{bmatrix} z^b_{y_2y_2} & z^b_{y_2y_6} & z^b_{y_2y_3} & z^b_{y_2y_5} \\ & z^b_{y_6y_6} & z^b_{y_6y_3} & z^b_{y_6y_5} \\ \text{Symmetric} & & z^b_{y_3y_3} & z^b_{y_3y_5} \\ & & & z^b_{y_5y_5} \end{bmatrix} .$$

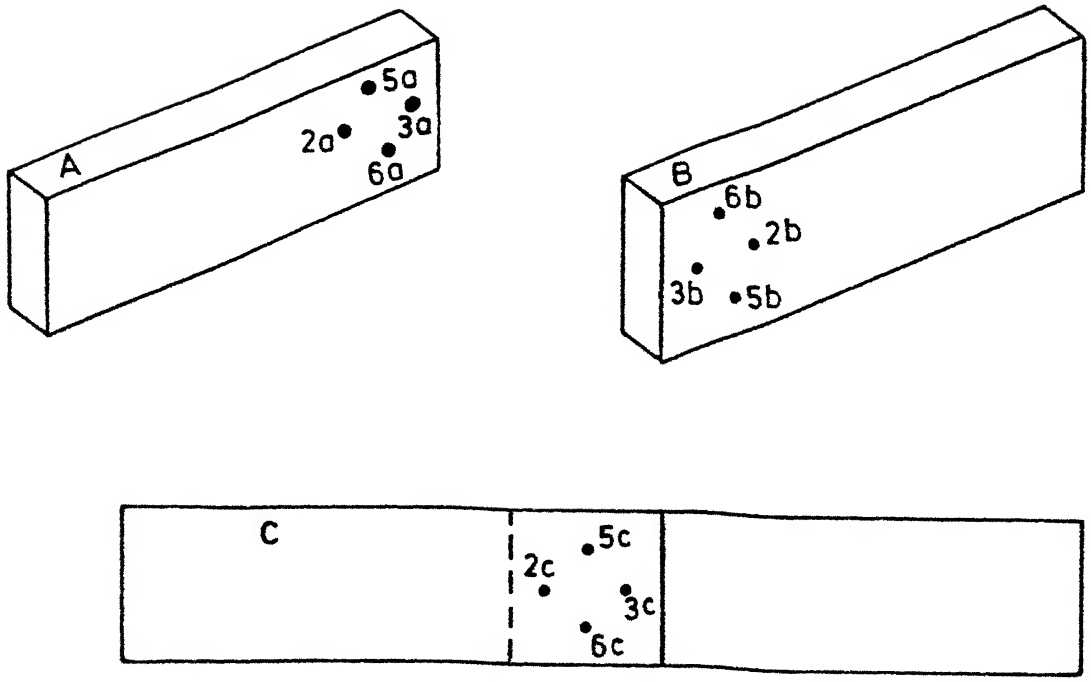

FIG. 3.5 FOUR-POINT ONE-dof MODEL

Noting the fact that the points 3,5,2,6 of beam A get coupled with the points 2,6,3,5 of beam B, the impedance matrix of the coupled structure can be written as,

$$[Z^c]_{y_3,y_5,y_2,y_6} = \begin{bmatrix} Z^a_{y_3y_3}+Z^b_{y_2y_2} & Z^a_{y_3y_5}+Z^b_{y_2y_6} & Z^a_{y_3y_2}+Z^b_{y_2y_3} & Z^a_{y_3y_6}+Z^b_{y_2y_5} \\ & Z^a_{y_5y_5}+Z^b_{y_6y_6} & Z^a_{y_5y_2}+Z^b_{y_6y_3} & Z^a_{y_5y_6}+Z^b_{y_6y_5} \\ \text{Symmetric} & & Z^a_{y_2y_2}+Z^b_{y_3y_3} & Z^a_{y_2y_6}+Z^b_{y_3y_5} \\ & & & Z^a_{y_6y_6}+Z^b_{y_5y_5} \end{bmatrix} \quad (3.18)$$

This model can account for coupling between bending and torsional oscillations.

3.3.4 One-point Two-dof Coupling:

While considering the bending oscillations, the eqilibrium conditions in coupling the two beams can be written in more precise terms if rotational coordinate is also assigned to the coupling point. This procedure is explained below.

The coupling coordinates considered for the substructures and for the coupled structure are shown in the Fig. 3.6(a). The rotational receptances required are calculated by reducing a linear parallel force system applied at two close points into a single force and moment system [8]. Fig. 3.6(b) shows the principle involved.

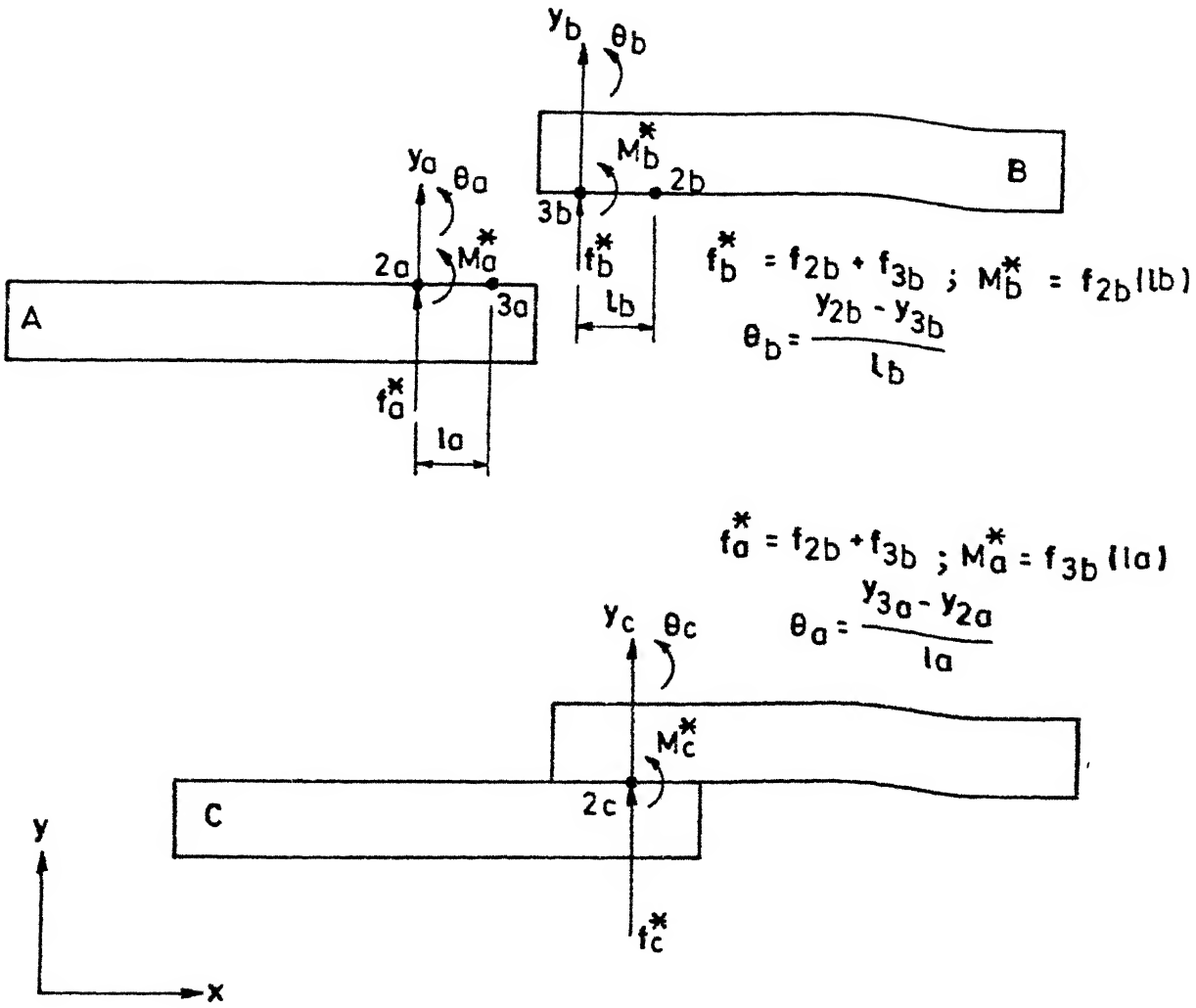

$$f_b^* = f_{2b} + f_{3b} \; ; \; M_b^* = f_{2b}(l_b)$$

$$\theta_b = \frac{y_{2b} - y_{3b}}{l_b}$$

$$f_a^* = f_{2b} + f_{3b} \; ; \; M_a^* = f_{3b}(l_a)$$

$$\theta_a = \frac{y_{3a} - y_{2a}}{l_a}$$

FIG. 3.6a ONE-POINT TWO-dof COUPLING MODEL

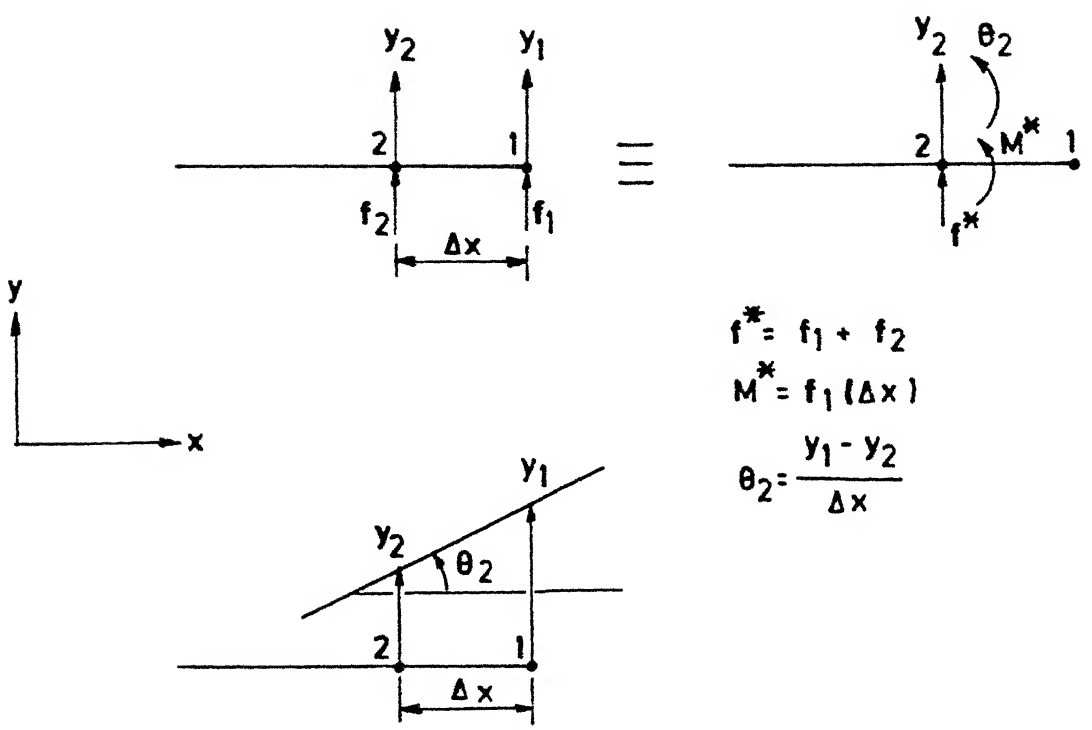

FIG. 3.6 (b) PRINCIPLE INVOLVED IN INTRODUCING ROTATIONAL COORDINATE

The receptances associated with rotations at the coupling point (i) are point receptances, namely, $\alpha_{y_i y_i}$ and $\alpha_{\theta_i \theta_i}$ and cross-point receptance, namely $\alpha_{y_i \theta_i}$. These are obtained in terms of substructure point receptances ($\alpha_{y_1 y_1}$ and $\alpha_{y_2 y_2}$) and transfer receptance ($\alpha_{y_1 y_2}$). The receptances $\alpha_{y_1 y_2}$ etc. can be measured directly using a single accelerometer. For this reason the receptances associated with rotatational dof i.e. $\alpha_{y_1 \theta_1}$ etc. are derived in terms of measured translational receptances $\alpha_{y_1 y_2}$ etc. as explained below. [For definition of various receptances [3] see Appendix B].

If the distance Δx (Fig. 3.6(b)) between the parallel lines of action of forces f_1 and f_2 is small enough, the system of forces (f_1, f_2) may be approximately reduced to an equivalent force-couple system at either point. If the equivalent force-couple system is considered at point 2, then the force at point 2 will be,

$$f^* = f_1 + f_2 \qquad (3.19(a))$$

and the couple will be

$$M^* = f_1(\Delta x) \qquad (3.19(b))$$

The rotation, at point 2 can be expressed as,

$$\theta_2 = \frac{y_1 - y_2}{\Delta x} \qquad (3.20)$$

Thus the two coordinates at point 2 are y_2 and θ_2. The objective is to obtain the receptances $\alpha_{\theta_2\theta_2}$ and $\alpha_{y_2\theta_2}$ so that the equivalent force and the equivalent moment can be used to write,

$$y_2 = \alpha_{y_2y_2} f^* + \alpha_{y_2\theta_2} M^* \tag{3.21}$$

and $$\theta_2 = \alpha_{y_2\theta_2} f^* + \alpha_{\theta_2\theta_2} M^*$$

The eqn. (3.19) can be used to express f_1 and f_2 in terms of f^* and M^* as

$$f_1 = M^*/\Delta x$$
$$f_2 = f^* - \frac{M^*}{\Delta x} \tag{3.22}$$

on the other hand y_1 and y_2 can also be written as

$$y_1 = \alpha_{y_1y_1} f_1 + \alpha_{y_1y_2} f_2$$
$$y_2 = \alpha_{y_1y_2} f_1 + \alpha_{y_2y_2} f_2 \tag{3.23}$$

Then eqns. (3.20), (3.22) and (3.23) can be arranged in the form of eqn. (3.21) such that,

$$\begin{bmatrix} y_2 \\ \theta_2 \end{bmatrix} = \begin{bmatrix} \alpha_{y_2y_2} & \dfrac{\alpha_{y_1y_2} - \alpha_{y_2y_2}}{\Delta x} \\ \dfrac{\alpha_{y_1y_2} - \alpha_{y_2y_2}}{\Delta x} & \dfrac{\alpha_{y_1y_1} + \alpha_{y_2y_2} - 2\alpha_{y_1y_2}}{(\Delta x)^2} \end{bmatrix} \begin{bmatrix} f^* \\ M^* \end{bmatrix} \tag{3.24}$$

or $$\{y\} = [\alpha]_{y_2,\theta_2} \{f\} \tag{3.25}$$

Figure (3.6(a)) shows the coupling of two substructures at points (2a, 3a) and (3b, 2b). This is considered as equivalent to one point coupling at point 2a and point 3b where two coordinates (i.e. translation and rotation) are associated with these points. In order to keep the same direction for rotation at point 3b and point 2a, we define,

$$\theta_b = \frac{y_{2b} - y_{3b}}{l_b} \quad \text{and} \quad \theta_a = \frac{y_{3a} - y_{2a}}{l_a}$$

$$M_b^* = f_{2b}(l_b) \quad \text{and} \quad M_a^* = f_{3b'}(l_a) \tag{3.26}$$

where the subscripts 'a' and 'b' refer to the substructures A and B respectively.

Eqn. (3.26) are used to express the receptance matrices for substructures A and B in the form of (3.25) as

$$\begin{bmatrix} y_a \\ \theta_a \end{bmatrix} = [\alpha^a] \begin{bmatrix} f_a^* \\ M_a^* \end{bmatrix} \quad \text{and} \begin{bmatrix} y_b \\ \theta_b \end{bmatrix} = [\alpha^b] \begin{bmatrix} f_b^* \\ M_b^* \end{bmatrix} \tag{3.27}$$

where,

$$[\alpha^a] = \begin{bmatrix} \alpha^a_{y_2y_2} & \dfrac{\alpha^a_{y_2y_3} - \alpha^a_{y_2y_2}}{l_a} \\ \dfrac{\alpha^a_{y_2y_3} - \alpha^a_{y_2y_2}}{l_a} & \dfrac{\alpha^a_{y_2y_2} + \alpha^a_{y_3y_3} - 2\alpha^a_{y_2y_3}}{l_a^2} \end{bmatrix} \tag{3.28}$$

$$[\alpha^b] = \begin{bmatrix} \alpha^b_{y_3y_3} & \dfrac{\alpha^b_{y_2y_3} - \alpha^b_{y_3y_3}}{l_b} \\ \dfrac{\alpha^b_{y_2y_3} - \alpha^b_{y_3y_3}}{l_b} & \dfrac{\alpha^b_{y_2y_2} + \alpha^b_{y_3y_3} - 2\alpha^b_{y_2y_3}}{l_b^2} \end{bmatrix}$$

The impedance matrix of the coupled structure (Fig. 3.6(a)) can be obtained in the form (from equation 3.12)

$$[Z^c]_{y_2,\theta_2} = \begin{bmatrix} Z^a_{y_2y_2} + Z^b_{y_3y_3} & Z^a_{y_2\theta_2} + Z^b_{y_3\theta_3} \\ Z^a_{y_2\theta_2} + Z^b_{y_3\theta_3} & Z^a_{\theta_2\theta_2} + Z^b_{\theta_3\theta_3} \end{bmatrix} \tag{3.29}$$

As an illustration for this model, the tip receptances, for the undamped free-free beam vibrations given by Bishop and Johnson [15] are used. The example cited here is for the coupling of two identical beam elements of properties detailed in Appendix A. The theoretical receptances and the receptance matrix for the coupled structure are given in Appendix C.

Figures 3.7(a), (b), (c) show the substructure (Appendix X, Fig. C.1) accelerances $\bar{a}_{y_1y_1}$, $\bar{a}_{y_1\theta_1}$ and $\bar{a}_{\theta_1\theta_1}$ respectively. The material damping is assumed to be zero. Figures 3.8(a) and (b) show the accelerance $\bar{a}^c_{y_1y_1}$ and $\bar{a}^c_{\theta_1\theta_1}$ at the coupling point of the coupled structure (Appendix C, Fig. C.2), respectively. These figures display accelerances rather than receptances. This is to maintain the uniformity with the results presented in Chapter 4, where the conversion from receptance to accelerance is also explained.

Another example is taken where the material damping is also considered. The formulas for calculating the point and transfer receptances (i.e. $\alpha_{y_2y_2}$, $\alpha_{y_2y_3}$ and $\alpha_{y_3y_3}$), as given by Snowdon [18], are given in the Appendix D. Coupling of two identical beams of Appendix A is considered and the rotational receptances (consisting of $\alpha_{y_2\theta_2}$)and $\alpha_{\theta_2\theta_2}$) are obtained in the form as given by equation (3.27). Then equation (3.29) is used to obtain the receptance for coupled structure. Figs. 3.9(a), (b) and (c) show $\bar{a}_{y_2y_2}$, $\bar{a}_{y_2y_3}$ and $\bar{a}_{y_3y_3}$ of the substructure accelerance and Figs. 3.10(a) and (b) show ($\bar{a}^c_{y_2y_2}$, $\bar{a}^c_{\theta_2\theta_2}$) and $\bar{a}^c_{y_2\theta_2}$ respectivel

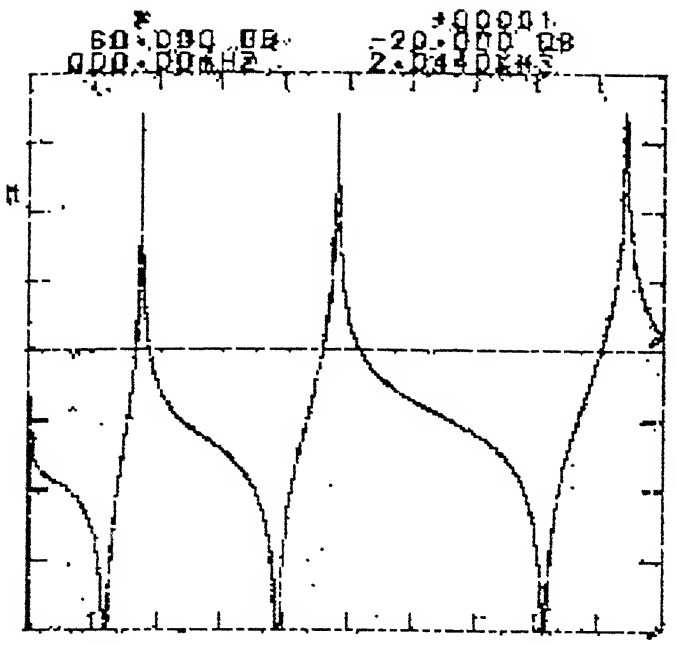

Fig.3.7(a): $|\bar{a}^{a}_{y_1 y_1}|$

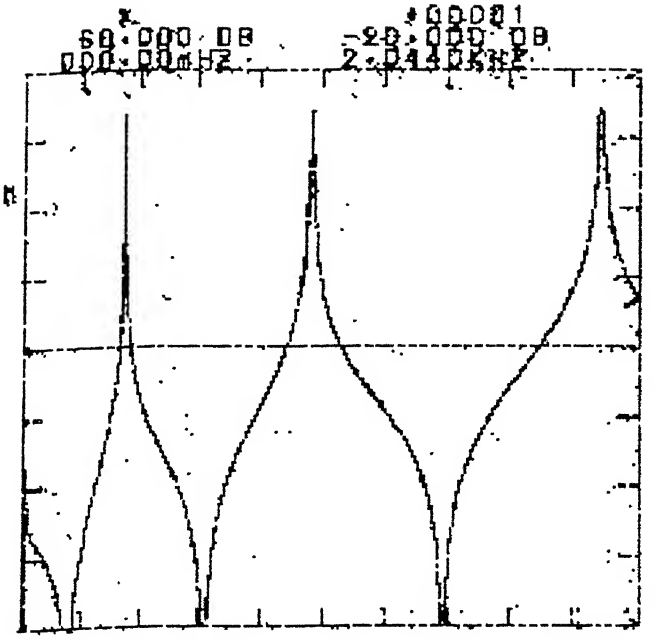

Fig. 3.7b : $|\bar{a}^{a}_{y_1 \theta_1}|$

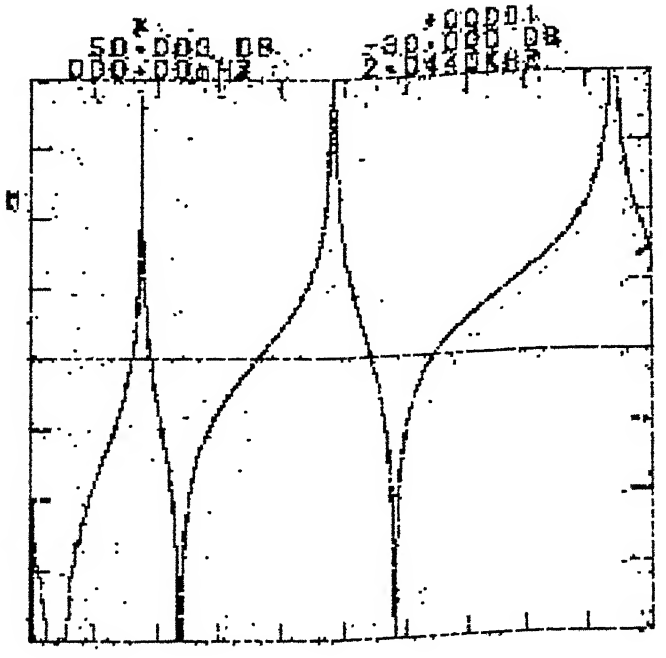

Fig. 3.7(c) : $|\bar{a}^{a}_{\theta_1 \theta_1}|$

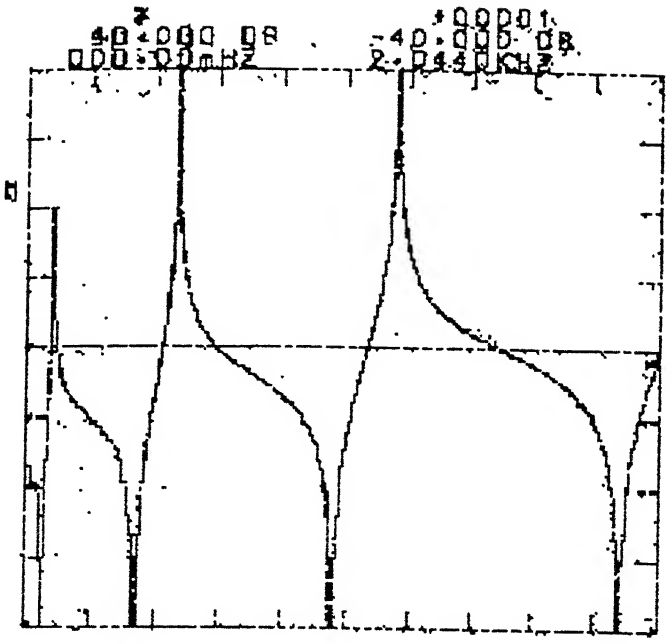

Fig.3.8(a): $|\bar{a}^{c}_{y_1 y_1}|$

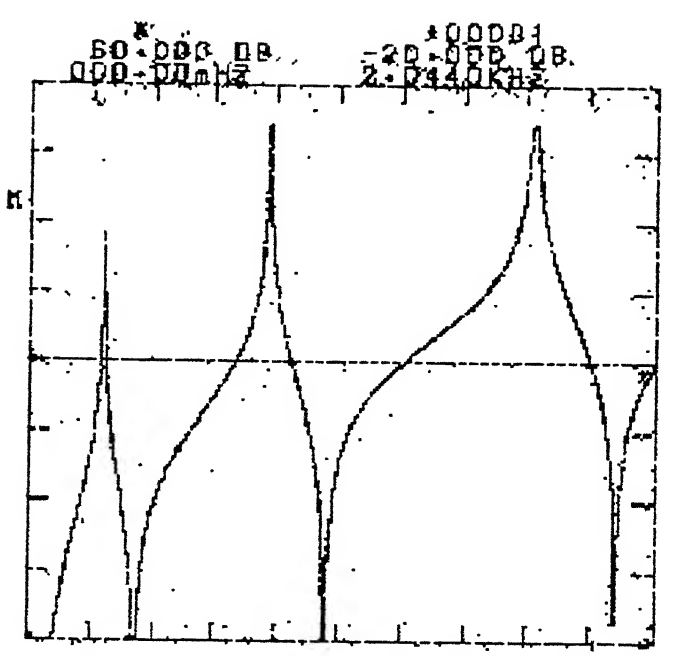

Fig. 3.8(b): $|\bar{a}^{c}_{\theta_1 \theta_1}|$

Fig. 3.8 : Theoretical FRFs of coupled structure (undamped system)

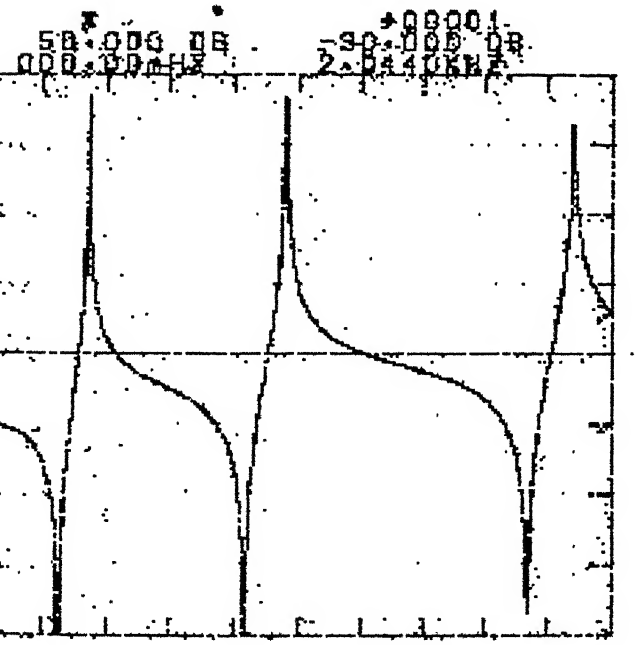

Fig.3.9(a) : $|\bar{a}^{a}_{y_2 y_2}|$

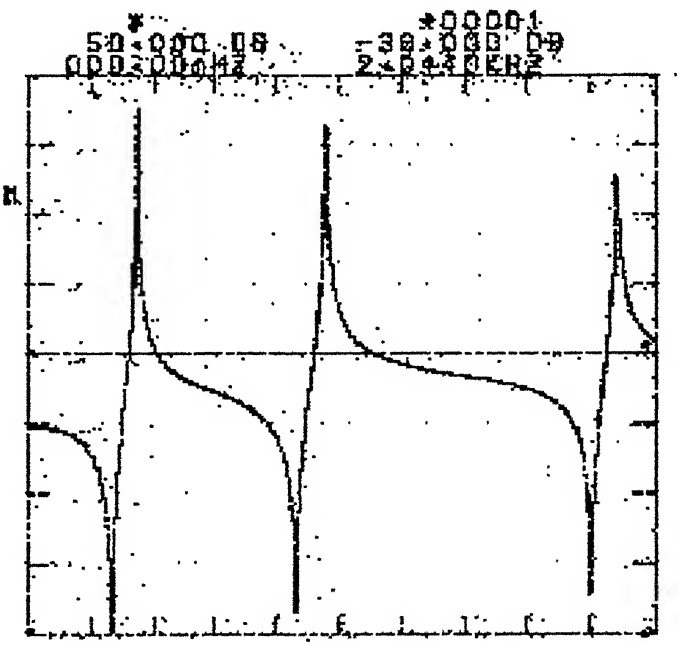

Fig.3.9(b) : $|\bar{a}^{a}_{y_2 y_3}|$

Fig. 3.9 : Theoretical FRFs of substructures (damped system)

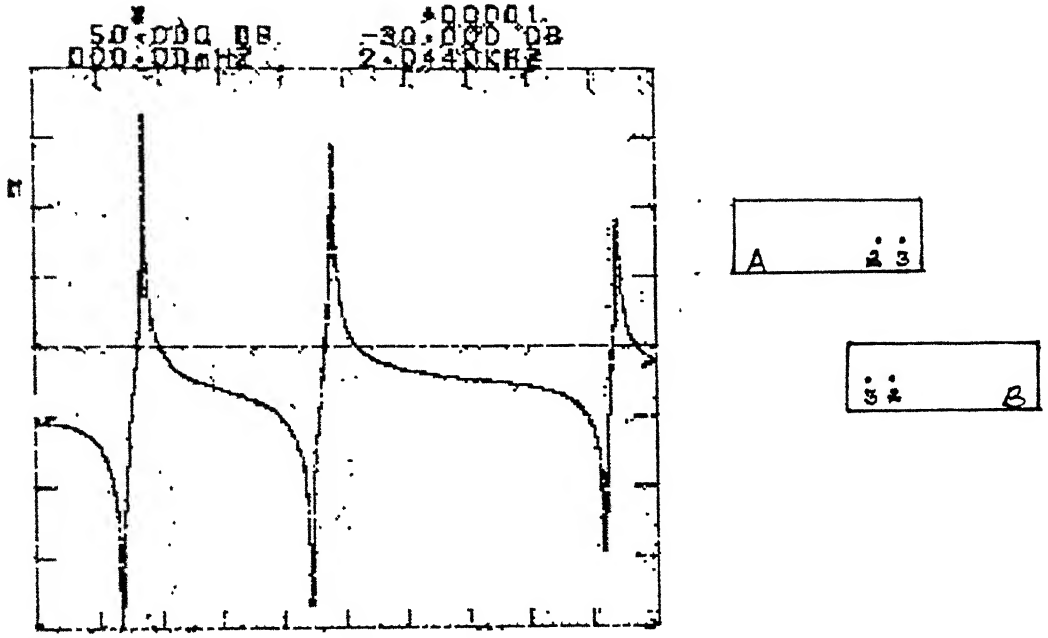

Fig. 3.9(c) : $|\bar{a}^{a}_{Y_3Y_3}|$

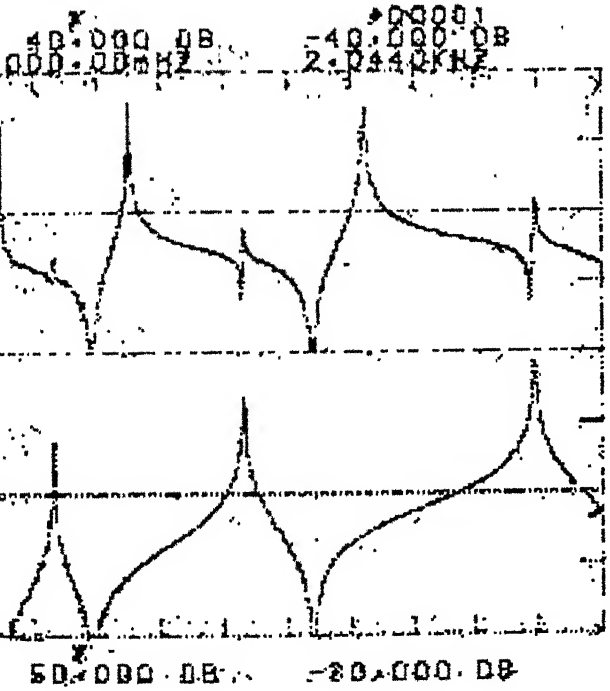

ig. 3.10(a): $|\bar{a}^{c}_{Y_2Y_2}|, |\bar{a}^{c}_{\theta_2\theta_2}|$

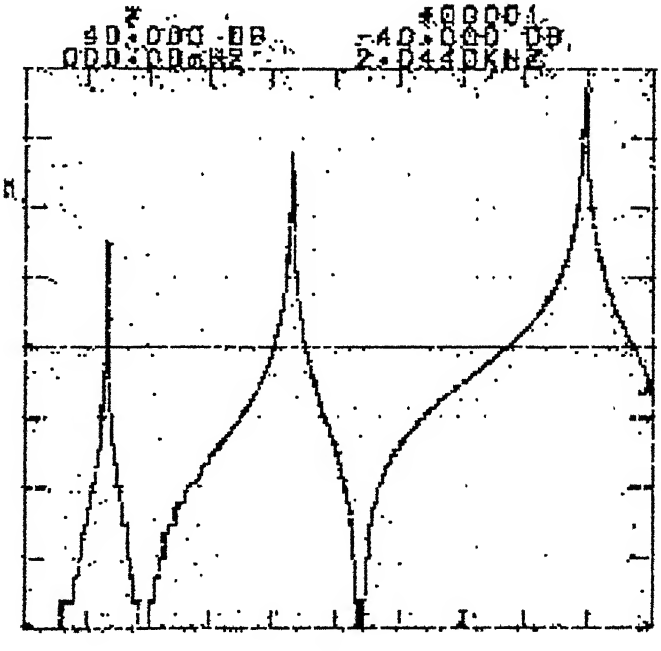

Fig.3.10(b) : $|\bar{a}^{c}_{Y_2\theta_2}|$

Fig. 3.10 : Theoretical FRFs of coupled structure (damped system)

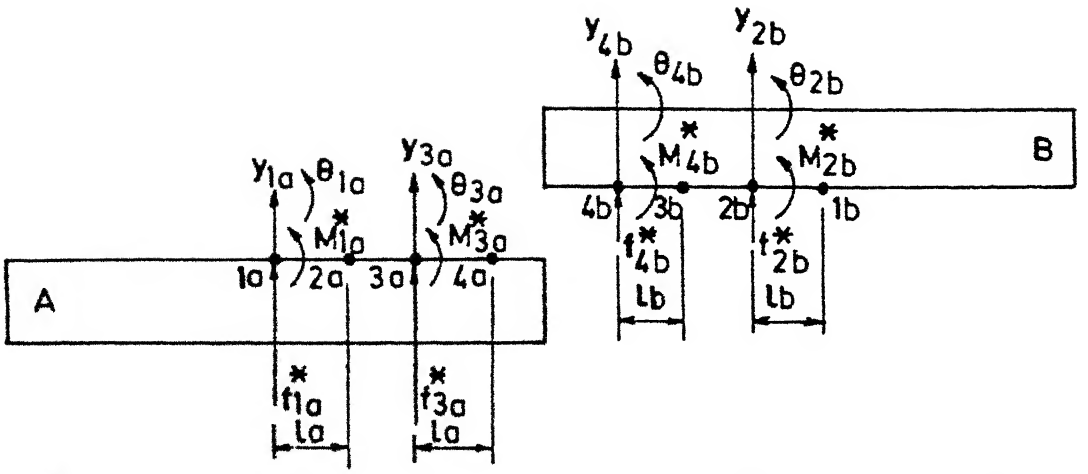

$f^*_{1a} = f_{1a} + f_{2a}$; $f^*_{3a} = f_{3a} + f_{4a}$

$M^*_{1a} = f_{2a}(la)$; $M^*_{3a} = f_{4a}(la)$

$$\theta_{1a} = \frac{y_{2a} - y_{1a}}{la} \quad ; \quad \theta_{3a} = \frac{y_{4a} - y_{3a}}{la}$$

$f^*_{2b} = f_{1b} + f_{2b}$; $f^*_{4b} = f_{3b} + f_{4b}$

$M^*_{2b} = f_{1b}(lb)$; $M^*_{4b} = f_{3b}(lb)$

$$\theta_{2b} = \frac{y_{1b} - y_{2b}}{lb} \quad ; \quad \theta_{4b} = \frac{y_{3b} - y_{4b}}{lb}$$

FIG. 3.11 (a)

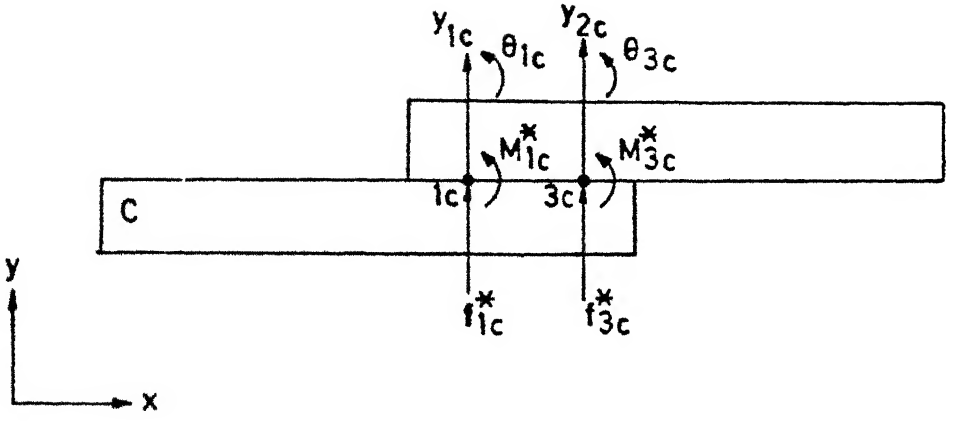

FIG. 3.11 (b) TWO-POINT TWO-dof COUPLING MODEL

3.3.4 Two-point Two-dof Coupling:

Figures 3.11(a) and (b) show the coupling coordinates considered on the substructure and the coupled structure. The parallel force systems acting at points (1a, 2a), (3a, 4a) on substructure A, (1b, 2b), (3b, 4b) on substructure B are reduced to an equivalent system of force and couple at points 1a, 3a on A and 2b and 4b on B respectively. Figure 3.11(a) also shows the expression for the equivalent force and moment. With these relations, the receptances involving rotation are written in terms of receptances for translation only. The procedure is as in section 3.3.4 and the obtained receptances are,

Elements of $[\alpha^a]_{y_1,\theta_1,y_3,\theta_3}$:

$$\alpha^a(1,1) = \alpha^a_{y_1y_1}$$

$$\alpha^a(1,2) = \frac{\alpha^a_{y_1y_2} - \alpha^a_{y_1y_1}}{l_a}$$

$$\alpha^a(1,3) = \alpha^a_{y_1y_3}$$

$$\alpha^a(1,4) = \frac{\alpha^a_{y_1y_4} - \alpha^a_{y_1y_3}}{l_a}$$

$$\alpha^a(2,2) = \frac{\alpha^a_{y_1y_1} + \alpha^a_{y_2y_2} - 2\alpha^a_{y_1y_2}}{l_a^2}$$

$$\alpha^a(2,3) = \frac{\alpha^a_{y_2y_3} - \alpha^a_{y_1y_3}}{l_a}$$

$$\alpha^a(2,4) = \frac{\alpha^a_{y_2y_4} - \alpha^a_{y_2y_3} + \alpha^a_{y_1y_3} - \alpha^a_{y_1y_4}}{l_a^2}$$

$$\alpha^a(3,3) = \alpha^a_{y_3y_3}$$

$$\alpha^a(3,4) = \frac{\alpha^a_{y_3y_4} - \alpha^a_{y_3y_3}}{l_a} \quad ; \quad a(4,4) = \frac{\alpha^a_{y_3y_3} + \alpha^a_{y_4y_4} - 2\alpha^a_{y_3y_4}}{l_a^2} \qquad (3.30)$$

Other elements can be obtained using the symmetricity of the receptance matrix.

Elements of $[\alpha^b]_{y_4,\theta_4,\ y_2,\theta_2}$:

$$\alpha^b(1,1) = \alpha^b_{y_4y_4}$$

$$\alpha^b(1,2) = \frac{\alpha^b_{y_3y_4} - \alpha^b_{y_4y_4}}{l_b}$$

$$\alpha^b(1,3) = \alpha^b_{y_2y_4}$$

$$\alpha^b(1,4) = \frac{\alpha^b_{y_1y_4} - \alpha^b_{y_2y_4}}{l_b}$$

$$\alpha^b(3,3) = \frac{\alpha^b_{y_3y_3} + \alpha^b_{y_4y_4} - 2\alpha^b_{y_3y_4}}{l_b^2}$$

$$\alpha^b(2,3) = \frac{\alpha^b_{y_2y_3} - \alpha^b_{y_2y_4}}{l_b}$$

$$\alpha^b(1,3) = \frac{\alpha^b_{y_1y_3} - \alpha^b_{y_2y_3} - \alpha^b_{y_1y_4} + \alpha^b_{y_2y_4}}{l_b}$$

$$\alpha^b(2,2) = \alpha^b_{y_2y_2}$$

$$\alpha^b(1,2) = \frac{\alpha^b_{y_1y_2} - \alpha^b_{y_2y_2}}{l_b}$$

$$\alpha^b(1,1) = \frac{\alpha^b_{y_1y_1} + \alpha^b_{y_2y_2} - 2\alpha^b_{y_1y_2}}{l_b^2} \qquad (3.31)$$

After this the impedance matrices of the substructure are calculated. These are coupled to get $[Z^c(\omega)]_{y_1,\theta_1,y_3,\theta_3}$ as

$$[Z^c(\omega)]_{y_1,\theta_1,y_3,\theta_3} = [Z^a(\omega)]_{y_1,\theta_1,y_3,\theta_3} \oplus [Z^b(\omega)]_{y_2,\theta_2,y_4,\theta_4} \qquad (3.32)$$

And finally the receptance matrix for the coupled structure is obtained by the inverting the impedance matrix of this coupled structure from (3.32).

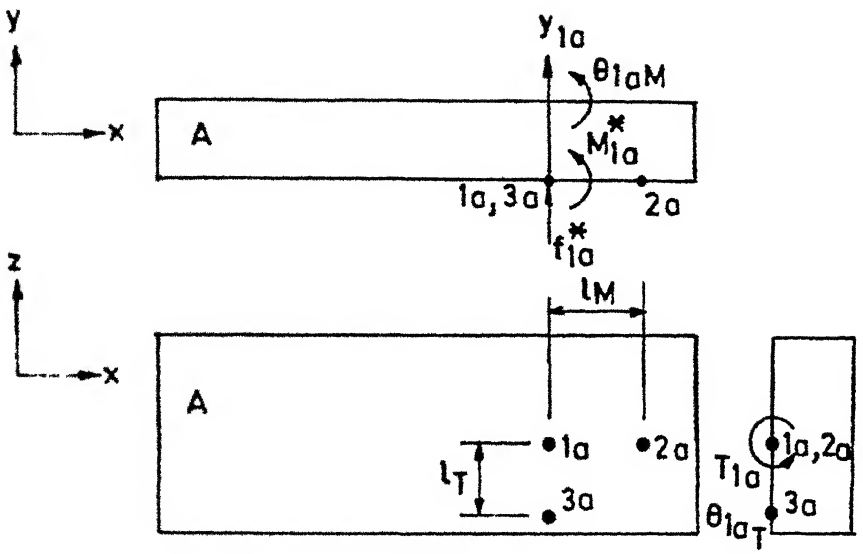

$$f^*_{1a} = f_{1a} + f_{2a} + f_{3a}$$

$$M^*_{1a} = f_{2a} l_M$$

$$T^*_{1a} = f_{3a} l_T$$

$$\theta_{1aM} = \frac{y_{2a} - y_{1a}}{l_M}$$

$$\theta_{1aT} = \frac{y_{3a} - y_{1a}}{l_T}$$

FIG. 3.12 (a)

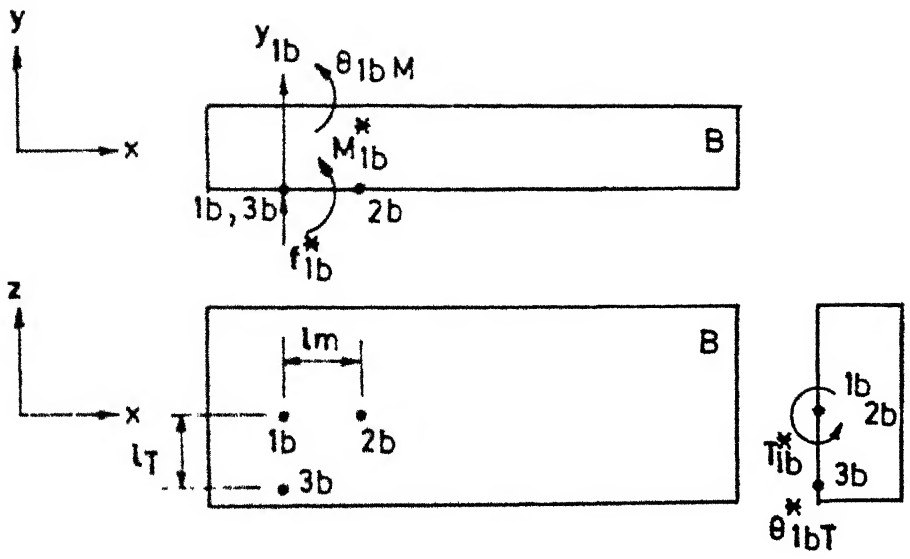

$$f^*_{1b} = f_b + f_{2b} + f_{3b}$$

$$M^*_{1b} = f_{2b}(l_m) \qquad \theta_{1bM} = \frac{y_{2b} - y_{1b}}{l_m}$$

$$T^*_{1b} = f_{3b}(l_T)$$

$$\theta_{1bT} = \frac{y_{3b} - y_{1b}}{l_T}$$

FIG. 3·12 (b)

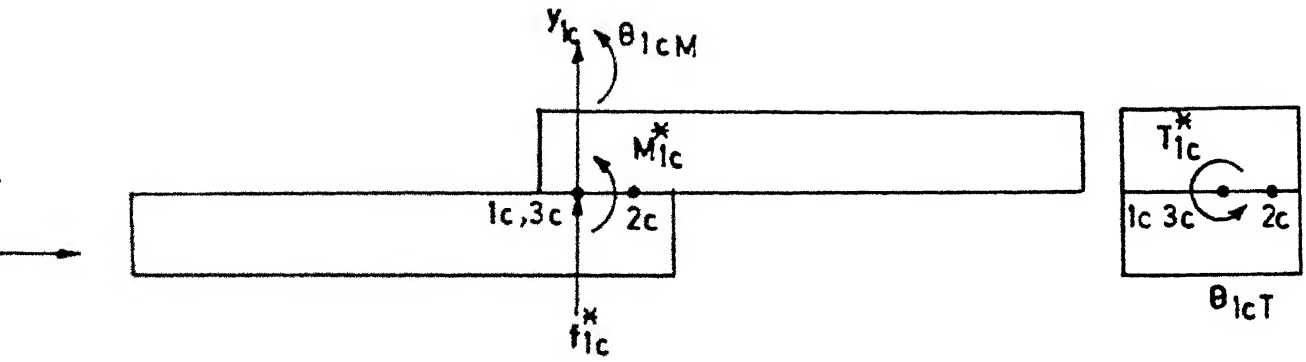

FIG. 3-12 (c)

ONE-POINT THREE-dof COUPLING MODEL

3.3.5 One-Point Three-dof Coupling:

If torsional vibrations were also found to be present in the structure, then the equilibrium conditions in coupling the two beams can be written in more precise terms if rotation associated with torsional vibration is also assigned to the coupling point. This procedure is explained below.

Figure 3.12(a) and (b) show the coordinates considered for reducing the parallel force system acting at points (1a,2a, 3a) and (1b, 2b, 3b) to an equivalent system of force, moment and torque at points 1a and 1b on the substructures A and B respectively. Figure 3.12(c) show the coupled structure and the coordinates associated with the coupling point.

Using the relations of equivalent force, moment and torque as given in Fig. 3.12(a) and (b), the substructure receptance matrices $[\alpha^a(\omega)]_{y_1,\theta_{1M},\theta_{1T}}$ and $[\alpha^b(\omega)]_{y_{11},\theta_{1M},\theta_{1T}}$ can be obtained in a similar way as explained in section 3.3.4. This yields,

Elements of $[\alpha^a]_{y_1,\theta_{1M},\theta_{1T}}$:

$$\alpha^a(1,1) = \alpha^a_{y_1y_1}$$

$$\alpha^a(1,2) = \frac{\alpha^a_{y_1y_2} - \alpha^a_{y_1y_1}}{l_M}$$

$$\alpha^a(1,3) = \frac{\alpha^a_{y_1y_3} - \alpha^a_{y_1y_1}}{l_T}$$

$$\alpha^a(2,2) = \frac{\alpha^a_{y_1y_1} + \alpha^a_{y_2y_2} - 2\alpha^a_{y_1y_2}}{l_M^2}$$

$$\alpha^a(2,3) = \frac{\alpha^a_{y_1y_1} - \alpha^a_{y_1y_3} + \alpha^a_{y_2y_3} - \alpha^a_{y_1y_2}}{l_M\, l_T}$$

$$\alpha^a(3,3) = \frac{\alpha^a_{y_1y_1} + \alpha^a_{y_3y_3} - 2\alpha^a_{y_1y_3}}{(l_T^2)} \qquad (3.33)$$

Elements of $[\alpha^b]_{y_1,\theta_{1M},\theta_{1T}}$:

$$\alpha^b(1,1) = \alpha^b_{y_1y_1}$$

$$\alpha^b(1,2) = \frac{\alpha^b_{y_1y_2} - \alpha^b_{y_1y_1}}{l_M}$$

$$\alpha^b(1,3) = \frac{\alpha^b_{y_1y_3} - \alpha^b_{y_1y_1}}{l_T}$$

$$\alpha^b(2,2) = \frac{\alpha^b_{y_1y_1} + \alpha^b_{y_2y_2} - 2\,\alpha^b_{y_1y_2}}{l_M^2}$$

$$\alpha^b(1,3) = \frac{\alpha^b_{y_1y_1} - \alpha^b_{y_1y_3} + \alpha^b_{y_2y_3} - \alpha^b_{y_1y_2}}{l_M l_T}$$

$$\alpha^b(3,3) = \frac{\alpha^b_{y_1y_1} + \alpha^b_{y_3y_3} - 2\alpha^b_{y_1y_3}}{l_T^2} \qquad (3.34)$$

These are used in the impedance coupling method for obtaining the receptance of the coupled structure as given below,

$$[Z^c(\omega)]_{y_1,\theta_{1M},\theta_{1T}} = [Z^a(\omega)]_{y_1,\theta_{1M},\theta_{1T}} \oplus [Z^b(\omega)]_{y_1,\theta_{1M},\theta_{1T}}$$

$$[\alpha^c(\omega)]_{y_1,\theta_{1M},\theta_{1T}} = [Z^c(\omega)]^{-1}_{y_1,\theta_{1M},\theta_{1T}} .$$

CHAPTER 4

EXPERIMENTAL RESULTS AND DISCUSSION

4.1 Introduction:

In this chapter, a brief explanation of the experimental setup and a procedure of testing adopted are given in section 4.2. The section 4.3 presents the predicted response of the coupled structure. Each subsection of 4.3 gives the results obtained from different coupling models. Substructures are analysed separately and the measured frequency data obtained from substructures are used to predict the response of the coupled structure. This is checked against the experimentally obtained FRF for the same coupled structure.

The FRF's displayed in this chapter are for accelerances ($\bar{a}$) but the modal parameters extraction are done from the receptance (α). The accelerance is measured instead of the required receptances. Receptances are calculated using,

$$\text{Accelerance, } \bar{a}_{jk}(\omega) = \frac{\hat{a}_j}{f_k} = -\omega^2 \alpha_{jk}(\omega) .$$

This additional computation required is due to the fact that the double integration process in charge amplifier results in the usage of high gain in amplifier which introduces noise. This can be clearly seen by observing coherence for both

accelerance and receptance measurement [1].

The measurements made on the test specimen (substructure or coupled structure) is for the free-free condition. The test specimen is hung over a frame using light strings to simulate the free-free condition.

4.2 Experimental Setup and Details of Testing:

The scheme of experimental setup is shown by the block diagram in Fig. 4.1. The instruments used in the present work are described briefly in the following.

Impact excitation using a hammer is a commonly used technique. Structures of masses 2 kg to 1000 kg can be excited by impact hammer. An impact hammer consists of different types of tips and heads for obtaining different frequency and force level ranges. Below the tip is a force transducer for detecting the magnitude of force of excitation. An impact hammer type 8202 (Brüel and Kjaer) is used in the present work.

Piezoelectric miniature accelerometer (B&K, type 4374) is used to pickup the response. An accelerometer is preferred over other types of pickups because of its smaller size and wider frequency range of operation. The miniature pickup has a mass of only 0.65 gm and with small dimensions (base diameter = 5 mm). It is suitable for measuring signals at closely placed locations.

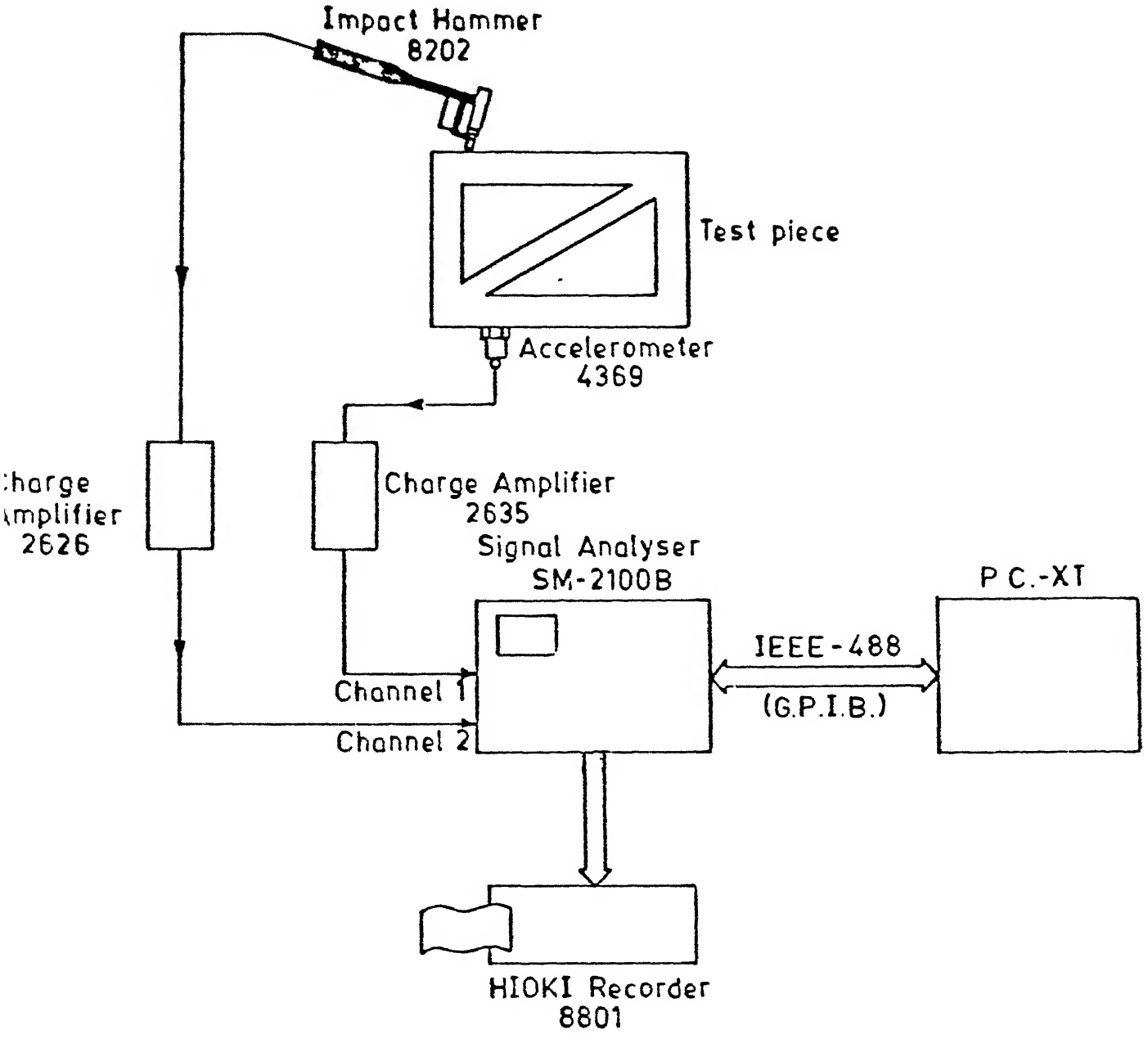

Block Diagram of Experimental Setup.

Fig. 4.1

Two charge amplifiers, one for response signal (B&K, type 2635) and the other for excitation signal (B&K, type 2626), are used to amplify weak signals into signals strong enough to be measured by the analyser.

The spectrum analyser receives two time signals, namely, the excitation and the response signals. The analyser operates on these signals to determine the system transfer-function or frequency response function. The operation performed on the two signals depends upon the function selected on the panel of the analyser. Analyser of type SM - 2100B (Iwatsu) is used in the present experimentation. Coherence function is selected as the operating function. The use of coherence function automatically calculates the auto-power, cross-power, coherence function and the transfer functions. These are registered in different memory blocks by the inbuilt functions.

The selection of frequency range and the data length decides the frequency resolution. Once the frequency range is selected, the data length can be selected depending upon the frequency resolution required.

In the post-processing (while extracting modal parameters) of the FRFs, the FRF data registered in the analyser is transferred to the IBM-PC/XT via GPIB (IEEE-488) bus. The data can also be sent back from PC to analyser. For taking hard copy print-outs of FRFs displayed on the CRT of the analyser, a

Memory Hi corder Type 8801 (Hioki) thermal plotter is used.

Some of the precautions to be taken while fetching the signals are noted below. The strength of the signal should be within the scale selected for the A/D converter of the analyser. Once the strength of the signals are set using amplifier, the A/D scale can then be set properly so that the signals lie within this scale. If this is not ensured then the digital data stored in the analyser memory will be faulty, i.e. the data gets clipped at the limiting value of the A/D converter scale.

A flat spectra of the force signal upto the frequency range of interest should be ensured. This can be achieved by proper selection of the tip of the impact hammer, by maintaining a correct duration of impact and by avoiding multiple hits. Flat nature of the autopower of the force signal indicates a correct impact.

The noise content of the signals should be kept minimum. By monitoring the coherence function, which should have a value of unity for good quality of signals, this can be achieved. High noise content in the region of antiresonance can be neglected as the data in this region is of not much importance in most of the experimentation.

Some of the limitations of the analyser may be noted. The unavailability of zoom facility causes difficulty in the extraction of modal parameters of lightly damped structures or

of weakly excited modes. If multichannel facility were available, then a good amount of measurement time can be saved especially when measurements at large number of co-ordinates are needed as in the case of two-dof and three-dof coupling models. The Iwatsu analyser provides only two types of windows namely rectangular and hanning windows. Rectangular window is used for both excitation (impulse) signal and response (transient) signal. Exponential window [3] would have been better for guiding the response signal as there is no windowing effect when a transient signal is guided through a rectangular window. The Iwatsu analyser does not permit the selection of independent windows for two channels.

4.3 Experimental Response of the Coupled Structures Vs. Predicted Response Using Impedance Coupling when the Substructures are Identical:

The coupling models discussed in Chapter 3 have been applied to the coupling of two identical beam elements. The substructures and the coupled structure along with their dimensions are shown in Fig. 4.2(a) and (b). The two beams are of MS and coupled at their one end using a bolt. A small washer was introduced between the two components to reduce the contact area within the experimental limits.

The response predicted using the various coupling models is compared with the directly measured experimental

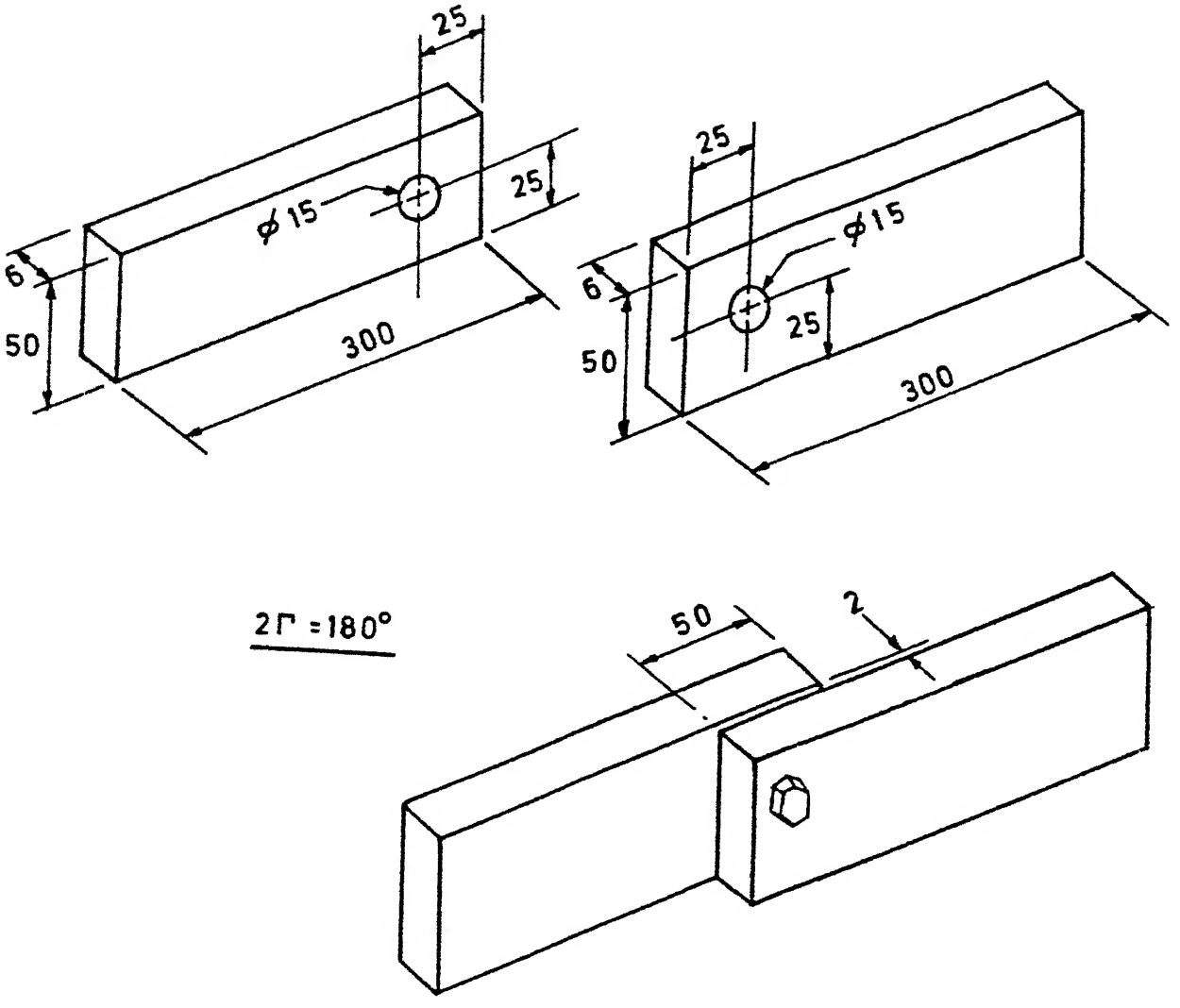

FIG. 4.2 a SUBSTRUCTURES AND THE COUPLED STRUCTURE

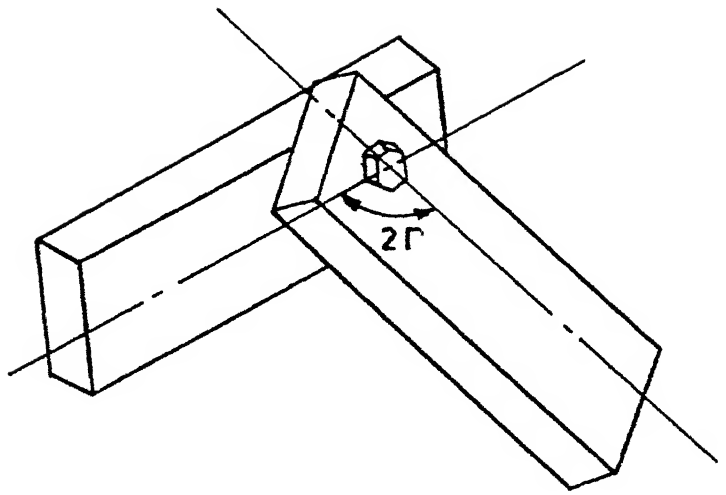

FIG. 4.2b COUPLED STRUCTURE AT $2\Gamma \neq 180^{\circ}$

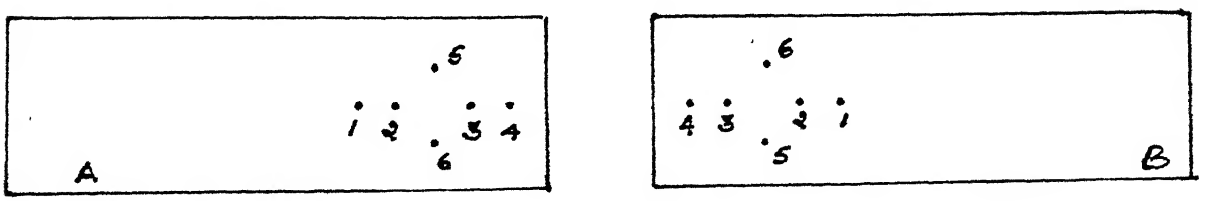

FIG 4.3

response from the coupled structure. The results were first compared for an included angle between the two beams of 180° ($\gamma = 180^{\circ}$). At this angle the torsional and bending vibrations are uncoupled.

4.3.1 Steps Involved in obtaining the Predicted Response of Coupled Structure:

The first step is to extract the modal parameters from the experimentally obtained FRFs of substructures. These modal parameters are used to regenerate the receptance of the substructures. The regenerated receptances are then used for predicting the response of coupled structure. Since the two substructure beams are identical, measurement on one beam is sufficient as long as the coupling points on both beams are on identical locations. The associated steps are better illustrated through examples. Thus the steps involved in obtaining the regenerated receptances $\alpha_{y_i y_j}$s(corresponding to translational coordinates only) are explained in section 4.3.2.1 and the steps involved in obtaining the regenerated $\alpha_{y_i \theta_j}$s (which corresponds to combined translational and rotational coordinates) are explained in section 4.3.2.3.

4.3.2 Predicted Response Through Different Coupling Models:

In the following sections the method involved in predicting the response of coupled structure using various models is explained.

4.3.2.1 Two-Point One-dof Coupling:

With reference to Fig. 4.3, the coupling points on substructures A and B for this model are assumed to be the points 2 and 3. The coupling is assumed to be at (A_2, B_3) and (A_3, B_2). The receptances to be used in equation (3.1) are the regenerated receptances. The procedure involved in obtaining the regenerated receptances is explained in the following.

The first step is to measure the substructure receptance $[\alpha^a(\omega)]_{y_2,y_3}$, which comprises of the point and transfer receptances measured at point 2 and 3. The single degree of freedom circle fit method [1] is used to extract the modal parameters from the experimentally obtained receptances. These modal parameters $({}_rA_{jk}, \omega_r, \eta_r)$ are then used in the equation

$$\alpha_{jk} = \sum_{r=1}^{N} \frac{{}_rA_{jk}}{(\omega_r^2 - \omega^2 + i\eta_r\omega_r^2)} \qquad (4.1)$$

to regenerate the receptances. The regenerated receptances are used rather than the measured ones to avoid the noise present in the experimentally measured receptances.

Figure 4.4 shows $\bar{a}_{y_3y_3}$ measured and regenerated substructure FRFs for a frequency range of 1 KHz. Figure 4.5(a) and Fig. 4.5(b) show $\bar{a}_{y_2y_3}$ and $\bar{a}_{y_2y_2}$ measured and regenerated substructure FRFs for a frequency range of 5 KHz. It can be seen from these figures that the regeneration is satisfactory and the modal parameters extracted are acceptable.

After obtaining the regenerated receptances, the next step is the calculation of substructure impedance matrices $[Z^a(\omega)]_{y_2,y_3}$ and $[Z^b(\omega)]_{y_2,y_3}$ as a function of frequency using equations (3.9) and (3.10). With the substructure being identical, the regenerated receptances of one beam are used for the other beam also. Therefore with the coupling points 2 and 3 in Fig. 4.3, the receptance matrices for beams A and B are related as:

$$\text{If } [\alpha^a] = \begin{bmatrix} \alpha_{22} & \alpha_{23} \\ \alpha_{23} & \alpha_{33} \end{bmatrix}, \text{ then } [\alpha^b] = \begin{bmatrix} \alpha_{33} & \alpha_{23} \\ \alpha_{23} & \alpha_{22} \end{bmatrix} \tag{4.2}$$

The complex inversion involved in obtaining impedance from receptance (or receptance from impedance) is carried out using the method given in Appendix E. The inversion is obtained at each frequency step over the frequency range considered.

The substructure impedance matrices are then coupled according to the equation (3.17) to obtain the impedance matrix $[Z^c(\omega)]_{y_2,y_3}$ of the coupled structure. The receptenace matrix

$[\alpha^2(\omega)]_{y_2,y_3}$ of the coupled is then obtained by inverting $[\beta^2(\omega)]_{y_2,y_3}$.

Using the procedure outlined above, the predicted response was obtained for frequency range of 1 KHz. Fig. 4.6(a) shows the predicted accelerance and the Fig. 4.6(b) shows the experimentally measured response of the coupled structure for 1 KHz frequency range. It is clear that the results of the predicted response are totally unsatisfactory. Moreover, the predicted receptance of coupled structure shows the peaks at the natural frequencies of the substructure (see Fig. 4.4). Measurement of response of the substructure over a wider frequency range results in inclusion of more number of modes and is expected to improve the results. Fig. 4.7(a) shows the predicted accelerance when the measurements were made upto 5 KHz (which includes upto 8 modes). It is observed that there is no improvement in the predicted response and the peaks still occur at the substructure natural frequencies. Fig. 4.7(b) shows the measured accelerance for the coupled structure for 5 KHz range.

4.3.2.2 Four-Point One-dof Coupling:

With reference to Figure 4.3, the coupling points on substructure A for this model are assumed to be the points 2,6,3 and 5. The corresponding coupling coordinates on substructure B are assumed to be the points 3,5,2 and 6. The

coupling is assumed to be at (A_2, B_3), (A_6, B_5), (A_3, B_2) and (A_5, B_6).

The regenerated receptances $[\alpha^a(\omega)]_{y_2,y_6,y_3,y_5}$ and $[\alpha^b(\omega)]_{y_3,y_5,y_2,y_6}$ are obtained in the similar way as explained in section 4.3.2.1. After this the impedance matrices $[Z^a(\omega)]_{y_2,y_6,y_3,y_5}$ and $[Z^b(\omega)]_{y_3,y_5,y_2,y_6}$ are calculated. These impedance matrices are coupled according to equation (3.18) to get $[Z^c(\omega)]_{y_2,y_6,y_3,y_5}$, which is then inverted to obtain $[\alpha^c(\omega)]_{y_2,y_6,y_3,y_5}$:

Figure 4.8 shows the measured and regenerated accelerances $\bar{a}_{y_6y_6}$, for a frequency range of 2 KHz. The modal parameter values of measured $\alpha_{y_6y_6}$ are listed in Table 4.1. Figure 4.9(a) shows the measured $\bar{a}^c_{y_2y_2}$ and Fig. 4.9(b) shows the predicted $\bar{a}^c_{y_2y_2}$ of the coupled structure. A careful study of Fig. 4.9(b) shows small blunt peaks at around 250 Hz, 450 Hz and 1200 Hz which happen to be the 2^{nd}, 3^{rd} and 6^{th} modes of the coupled structure. But since all the substructure natural frequencies have reappeared in the predicted response, the prediction is still not a good representation of the coupled structure response.

4.3.2.3 <u>One Point Two-dof Coupling:</u>

In this model the coupling is assumed to be on a single point (A_2, B_3) (Fig. 4.3) and two coordinates y_2 and θ_2 are associated with this point. Initially the receptances

Table 4.1 : Modal Parameter of Substructure (Torsional Mode Considered)

FRF	Mode	Natural frequency	Damping loss factor %	Real part of Modal constant	Imaginary part of modal constant
$\alpha_{y_6 y_6}$	1	354	0.029	-0.346499	-0.220731
	2	966	0.02	-0.053238	-0.062875
	3	1242	0.043	-0.544785	+0.000433
	4	1878	0.049	-0.004910	0.001175

$\alpha_{y_2y_2}$, $\alpha_{y_2y_3}$, $\alpha_{y_3y_3}$ are measured at 2 and 3. These are then regenerated as explained in section 4.3.2.1. The regenerated FRFs are used to obtain $[\alpha^a(\omega)]_{y_2,\theta_2}$ and $[\alpha^b(\omega)]_{y_3,\theta_3}$ as explained in section 3.3.4 of Chapter 3. The distance between the parallel lines of action of forces is taken as 25 mm. $[\alpha^a(\omega)]_{y_2,\theta_2}$ and $[\alpha^b(\omega)]_{y_3,\theta_3}$ are inverted to give $[Z^a(\omega)]_{y_2,\theta_2}$ and $[Z^b(\omega)]_{y_3,\theta_3}$. These impedance matrices are then coupled according to equation (3.29) to get $[Z^c(\omega)]_{y_2,\theta_2}$ which is then inverted to get $[\alpha^c(\omega)]_{y_2,\theta_2}$. Table 4.2 shows one set of sample calculation at ω = 356 Hz (first natural frequency of the substructure).

Figure 4.10 shows the measured $\bar{a}^a_{y_2y_2}$ (torsional mode, ω = 1242 Hz, is not considered in regeneration) and Fig. 4.11 show predicted $\bar{a}^c_{y_2y_2}$ and $\bar{a}^c_{\theta_2\theta_2}$ for 2 KHz frequency range. Eventhough a direct comparison between $\alpha^c_{y_2y_2}$ (experimentally measured) and $\alpha^c_{\theta_2\theta_2}$ (predicted) is not true indication of quantitative differences, the inferences about natural frequencies can be made. From the Figure 4.11, it can be noted that there is no improvement in the predicted response, as all the substructure natural frequencies have reappeared very prominently. A very small peak can be noted near the second natural frequency of the coupled structure.

Table 4.2 : Values of Receptances and Impedances of Substructures and Coupled Structure at a Frequency of 356 Hz
(The distance between two points 2 and 3 = 0.025 m)

(i) Regenerated receptance : $[\alpha^a(\omega)]_{y_2,y_3}$

FRF	Real part	Imaginary part
$\alpha_{y_2y_2}$	1.654×10^{-6}	1.905×10^{-6}
$\alpha_{y_2y_3}$	1.915×10^{-6}	1.925×10^{-6}
$\alpha_{y_3y_3}$	5.155×10^{-6}	3.815×10^{-6}

(ii) $[\alpha^a(\omega)]_{y_2,\theta_2}$ and $[Z^a(\omega)]_{y_2,\theta_2}$:

(a) Receptance

FRF	Real part	Imaginary part
$\alpha_{y_2y_2}$	1.654×10^{-6}	1.905×10^{-6}
$\alpha_{y_2\theta_2}$	1.046×10^{-5}	8.000×10^{-7}
$\alpha_{\theta_2\theta_2}$	4.765×10^{-3}	2.994×10^{-3}

Continued....

Table 4.8 (Continued):

(b) Impedance

FRF	Real part	Imaginary part
$Z_{y_2y_2}$	$2.583\text{x}10^{5}$	$-3.019\text{x}10^{5}$
$Z_{y_2\theta_2}$	$-1.638\text{x}10^{2}$	$7.221\text{x}10^{2}$
$Z_{\theta_2\theta_2}$	$1.501\text{x}10^{2}$	$-9.587\text{x}10$

(iii) $[\alpha^b(\omega)]_{y_3,\theta_3}$ and $[Z^b(\omega)]_{y_3,\theta_3}$:

(a) Receptance

FRF	Real part	Imaginary part
$\alpha_{y_3y_3}$	$5.155\text{x}10^{-6}$	$3.816\text{x}10^{-6}$
$\alpha_{y_3\theta_3}$	$1.296\text{x}10^{-4}$	$7.565\text{x}10^{-5}$
$\alpha_{\theta_3\theta_3}$	$4.765\text{x}10^{-3}$	$2.994\text{x}10^{-3}$

(b) Impedance

FRF	Real part	Imaginary part
$Z_{y_3y_3}$	$2.583\text{x}10^{5}$	$-3.019\text{x}10^{5}$
$Z_{y_3\theta_3}$	$-6.621\text{x}10^{3}$	$8.272\text{x}10^{3}$
$Z_{\theta_3\theta_3}$	$3.197\text{x}10^{2}$	$-3.207\text{x}10^{2}$

Continued....

(iv) $[Z^c(\omega)]_{y_2,\theta_2}$ and $[\alpha^c(\omega)]_{y_2,\theta_2}$:

(a) Impedance

FRF	Real part	Imaginary part
$Z_{y_2y_2}$	5.166×10^{5}	-6.039×10^{5}
$Z_{y_2\theta_2}$	-6.785×10^{3}	8.994×10^{3}
$Z_{\theta_2\theta_2}$	4.698×10^{2}	-4.166×10^{2}

(b) Receptance

FRF	Real part	Imaginary part
$\alpha_{y_2y_2}$	1.186×10^{-6}	1.165×10^{-6}
$\alpha_{y_2\theta_2}$	2.498×10^{-5}	1.628×10^{-5}
$\alpha_{\theta_2\theta_2}$	1.689×10^{-3}	1.254×10^{-3}

4.3.2.4 Two-Point Two-dof Coupling:

In this model the coupling is assumed to be at (A_1, B_4) and (A_3, B_2) (Fig. 4.3) and the coordinates (y_1, θ_1) and (y_3, θ_3) are associated with these points. The distance between the parallel lines of action of forces (required for calculating the equivalent moment) is taken as 10 mm. $[Z^a(\omega)]_{y_1,\theta_1,y_3,\theta_3}$ and $[Z^b(\omega)]_{y_2,\theta_2,y_4,\theta_4}$ are obtained by inverting $[\alpha^a(\omega)]_{y_1,\theta_1,y_3,\theta_3}$ and $[\alpha^b(\omega)]_{y_2,\theta_2,y_4,\theta_4}$, respectively. These impedance matrices are then coupled to get the impedance matrix of the coupled structure which is inverted to get the receptance matrix of the coupled structure according to equation (3.32).

Some of the measured and regenerated substructure FRFs are superimposed in Fig. 4.12, for a frequency range of 2 KHz. The effect of torsional mode on the receptance is very small as this is very weakly excited for this set of points 1,2,3 and 4 lying on the center line. Therefore, the torsional mode (natural frequency = 1242 Hz) is not considered while regeneration. This can be seen by looking at the regenerated FRFs in Fig. 4.12, which does not show a peak at ω= 1242 Hz. Table 4.3 gives the modal parameter values for the FRFs shown in Fig. 4.12. Fig. 4.13 (a) and 4.13(b) shows substructure $\bar{a}^b_{y_2\theta_2}$ and $\bar{a}^b_{\theta_2\theta_2}$ for 2 KHz frequency range as calculated from equation (3.24). The general nature of these FRFs is still same as those shown in Fig. 4.12.

Table 4.3 : Modal Parameters of Substructure

FRF	Mode	Natural frequency	Damping loss factor %	Real part of Modal constant	Imaginary part of Modal constant
$\alpha_{y_1y_1}$	1	354	0.036	-0.062054	-0.057178
	2	966	0.018	-0.00149	-0.002459
	3	1878	0.032	-0.149967	0.013547
$\alpha_{y_1y_2}$	1	354	0.026	-0.105826	-0.109773
	2	966	0.063	+0.004608	+0.004718
	3	1878	0.036	-0.097786	0.023919
$\alpha_{y_3y_3}$	1	354	0.027	-0.293307	-0.205255
	2	966	0.036	-0.145475	-0.080370
	3	1878	0.046	-0.074309	0.047883
$\alpha_{y_3y_3}$	1	354	0.026	-0.454415	-0.159304
	2	966	0.037	-0.112060	-0.290572
	3	1878	0.048	-0.211499	-0.026388

Figure 4.14(a), (b) and (c) show predicted $\bar{a}^c_{y_3\theta_1}$, $\bar{a}^c_{\theta_1\,\theta_3}$ and $\bar{a}^c_{\theta_3\,\theta_3}$ of the coupled structure, respectively. A small peak at around 250 Hz corresponding to 2nd mode of coupled structure has appeared in the predicted response. But the prodiction is not good as all the substructure natural frequencies have reappeared very prominantly.

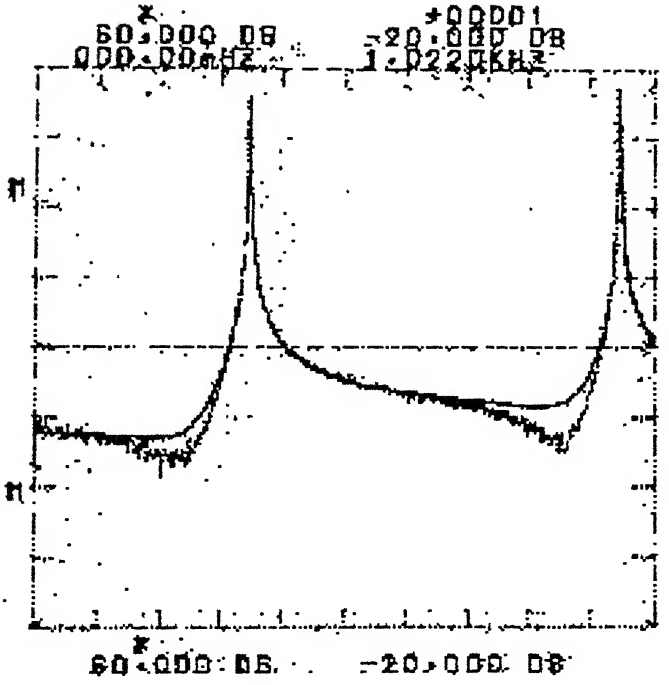

Fig. 4.4 : $|\bar{a}_{y_3y_3}|$

Fig. 4.4 : Measured and regenerated substructure FRF (1 KHz range)

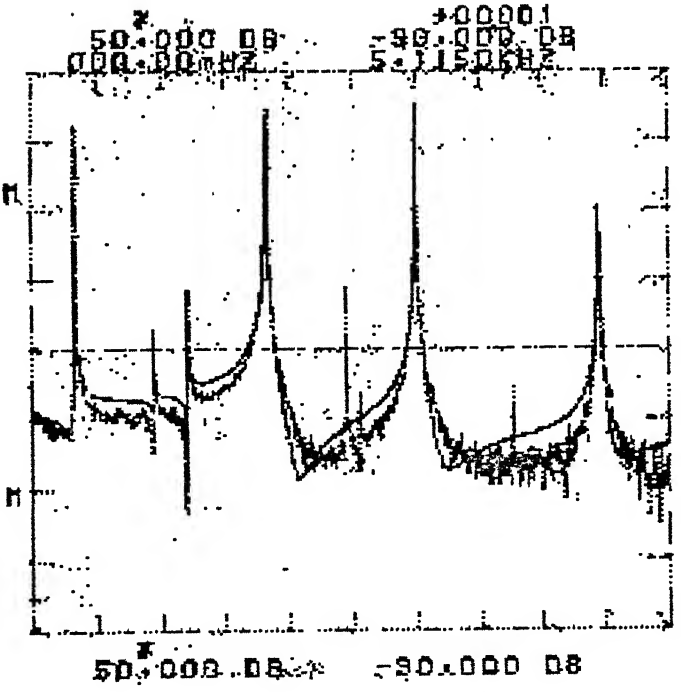

Fig.4.5(a): $|\bar{a}_{y_2y_3}|$

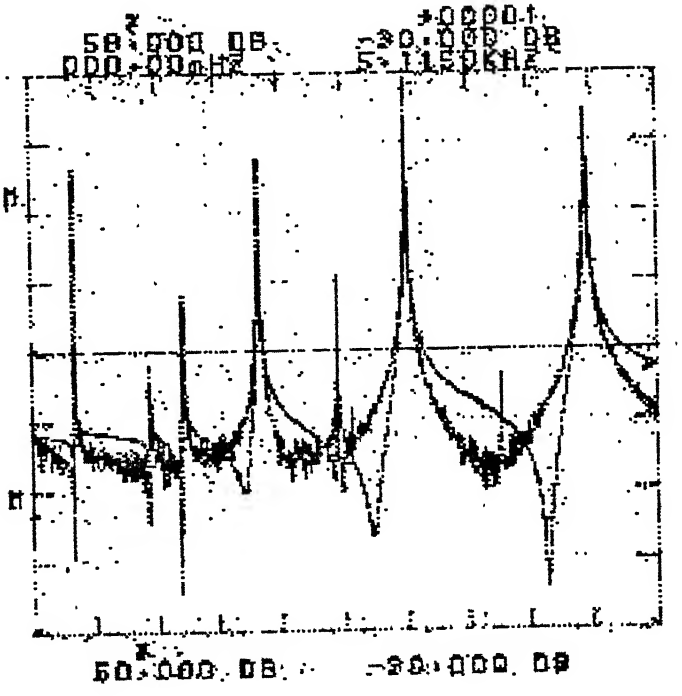

Fig.4.5(b): $|\bar{a}_{y_2y_2}|$

Fig. 4.5: Measured and regenerated substructure FRF (5 KHz range)

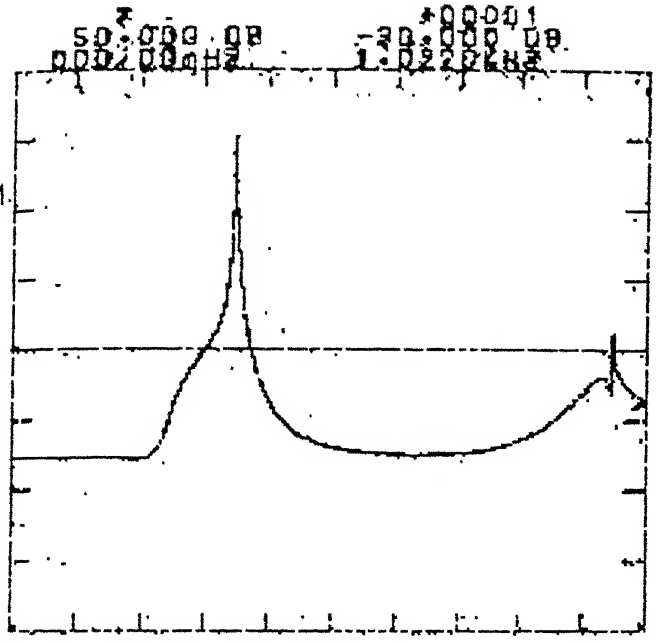

Fig.4.6(a): $|\bar{a}^{c}_{y_2y_2}|$

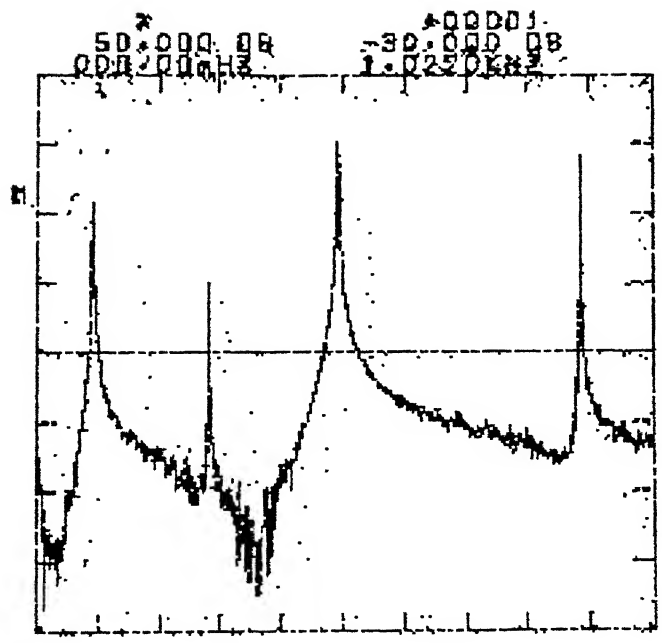

Fig.4.6(b) : $|\bar{a}^{c}_{y_2y_2}|$

Fig.4.6: Two-point One-dof coupling: Predicted and measured response of coupled structure (1 KHz range)

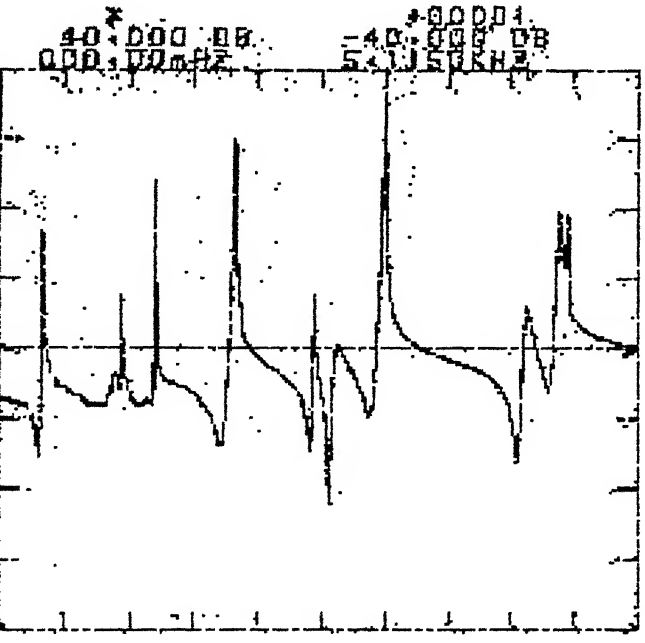

4.7(a) : $|\bar{a}^{c}_{yy}|$

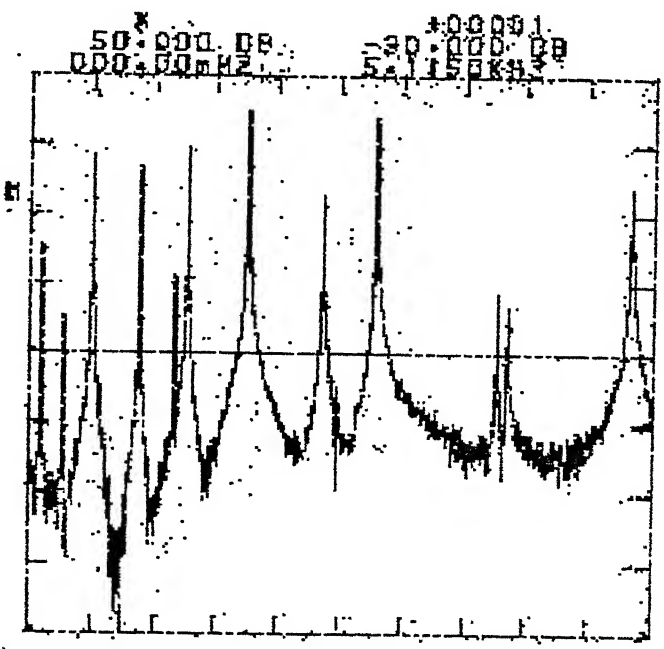

Fig. 4.7(b): $|\bar{a}^{c}_{yy}|$

Fig.4.7: Two-point One-dof coupling: Predicted and measured response of coupled structure (5 KHz range)

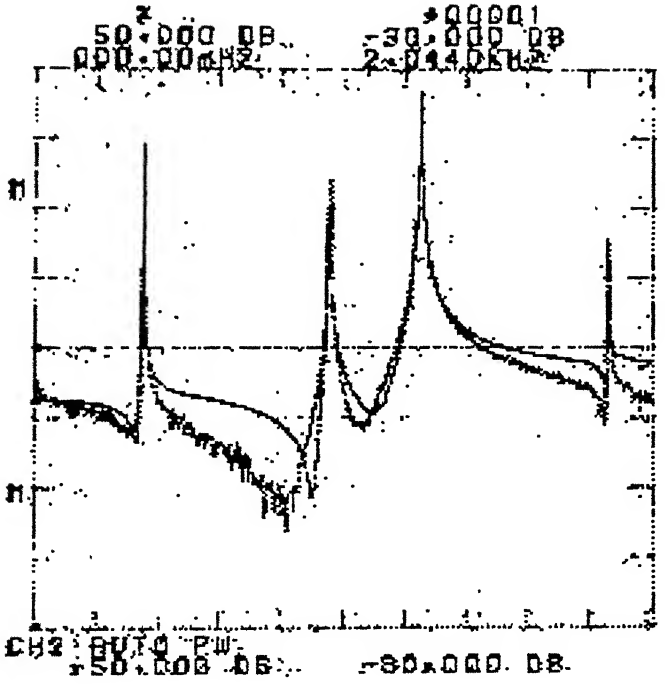

Fig. 4.8(a) : $|\bar{a}^{a}_{y_6 y_6}|$

Fig. 4.8 : Measured and regenerated substructure FRF of a point situated off the centre line

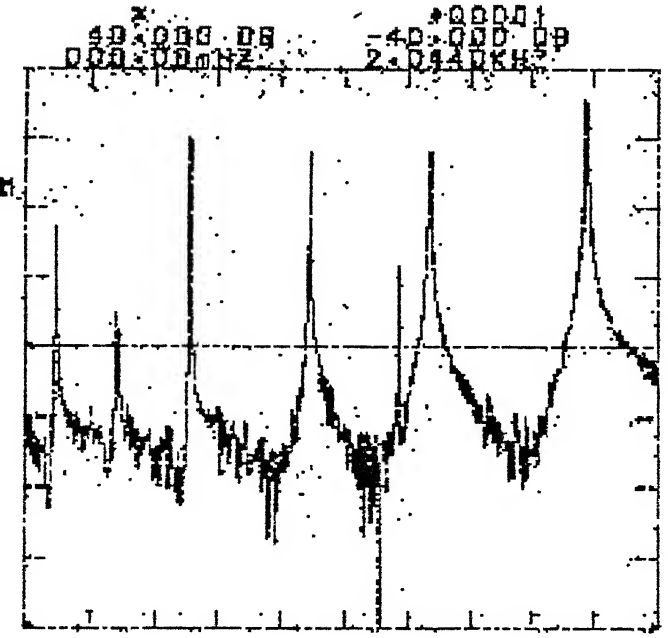

Fig. 4.9(a): $|\bar{a}^{c}_{y_2 y_2}|$

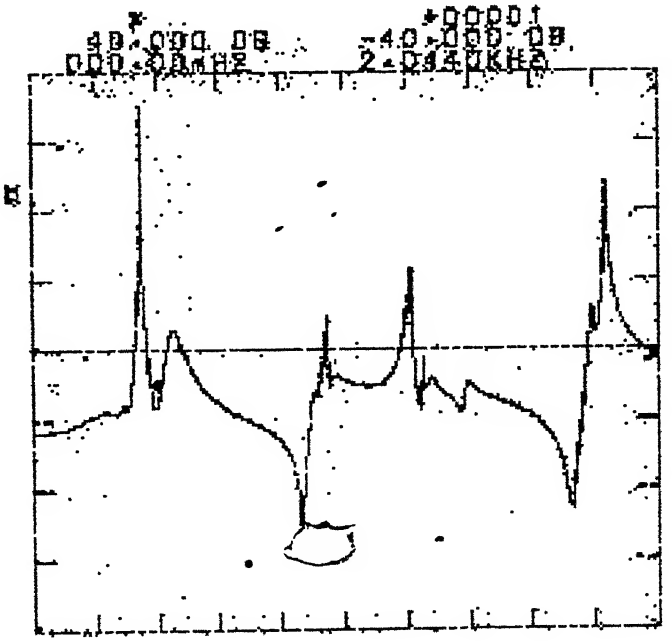

Fig. 4.9(b) : $|\bar{a}^{c}_{y_2 y_2}|$

Fig. 4.9: Four-point One-dof coupling: Measured and predicted

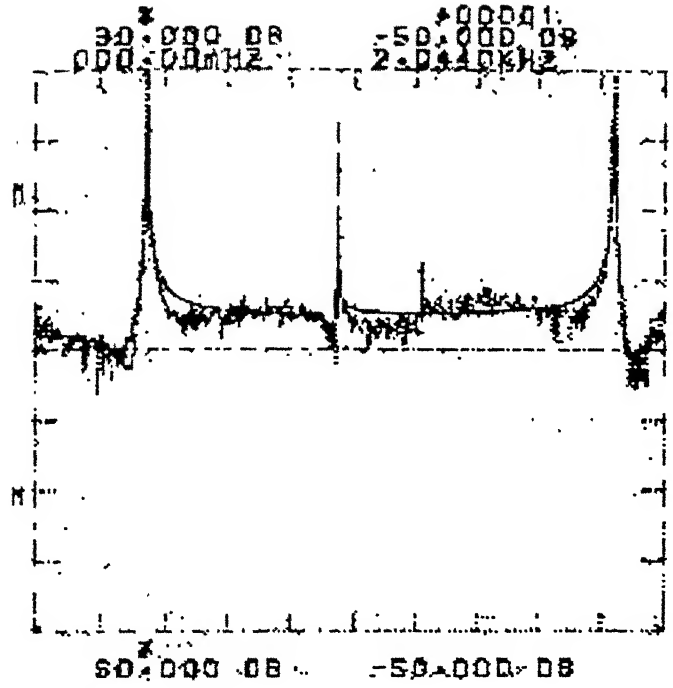

Fig. 4.10: $|\bar{a}^{a}_{y_2y_2}|$

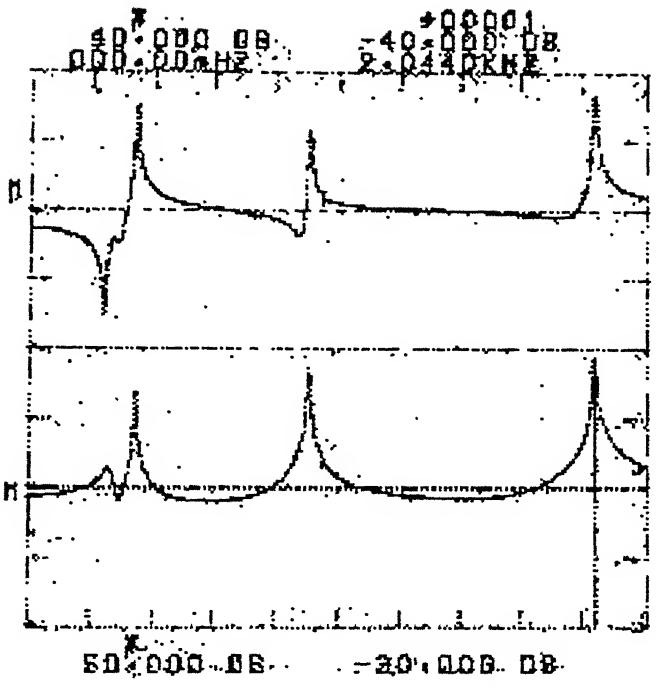

Fig. 4.11: $|\bar{a}^{c}_{y_2y_2}|, |\bar{a}^{c}_{\theta_2\theta_2}|$

g.4.10 & Fig. 4.11 : One-point Two-dof coupling: Measured and predicted response of coupled structure

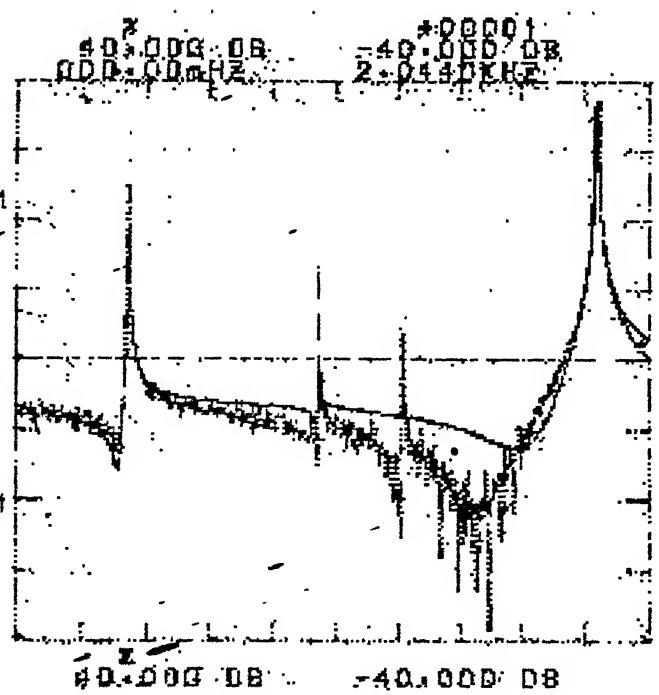

Fig. 4.12 : $|\bar{a}^{a}_{y_1y_1}|$

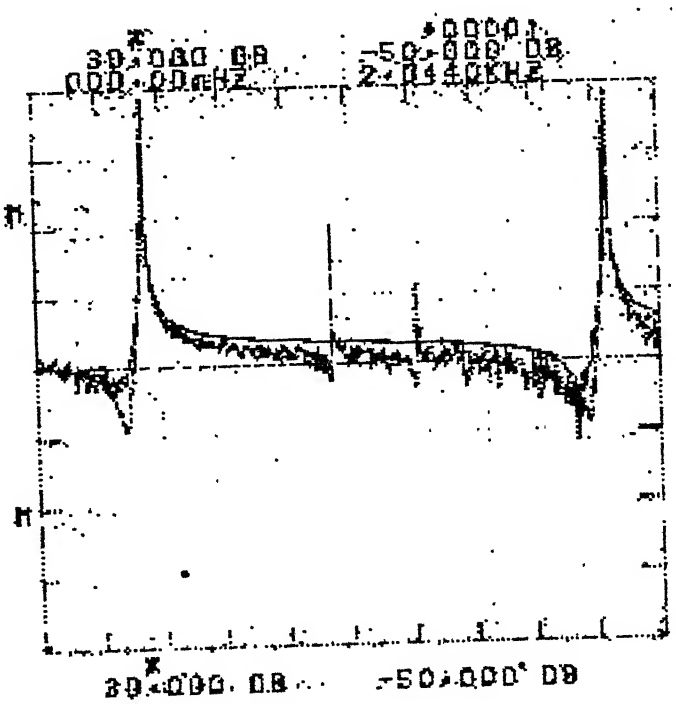

Fig.4.12: $|\bar{a}^{a}_{y_1y_2}|$

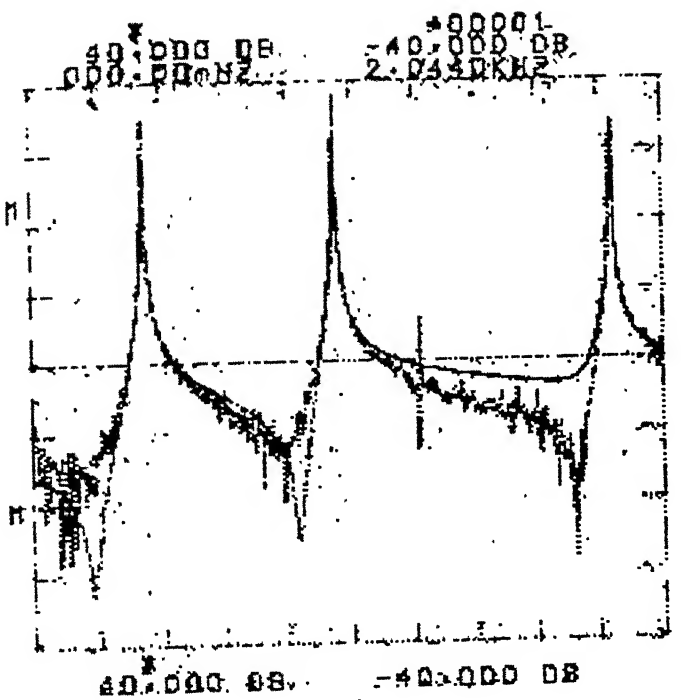

Fig. 4.12 : $|\bar{a}^{a}_{y_3,y_3}|$

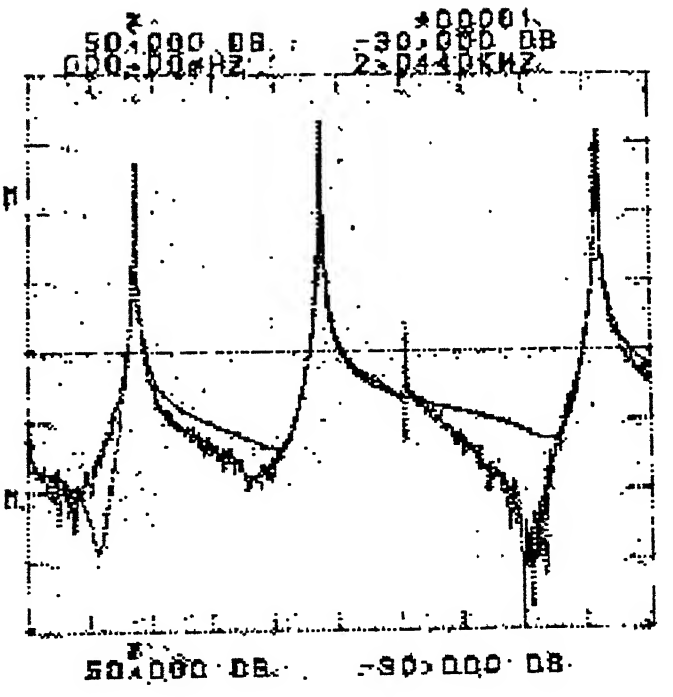

Fig. 4.12: $|\bar{a}^{a}_{y_3y_4}|$

Fig.4.12 : Meaaured and regenerated substructure FRFs.

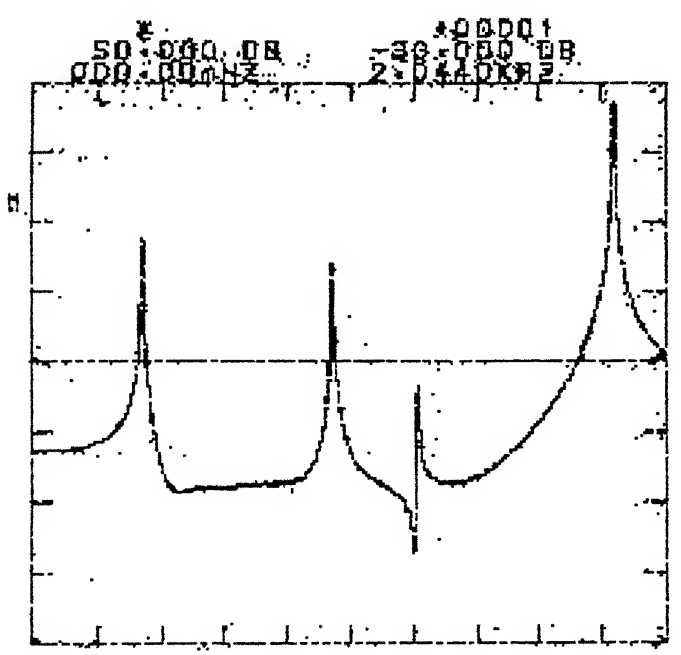

Fig.4.13(a) : $|\bar{a}^{a}_{y_3\theta_2}|$

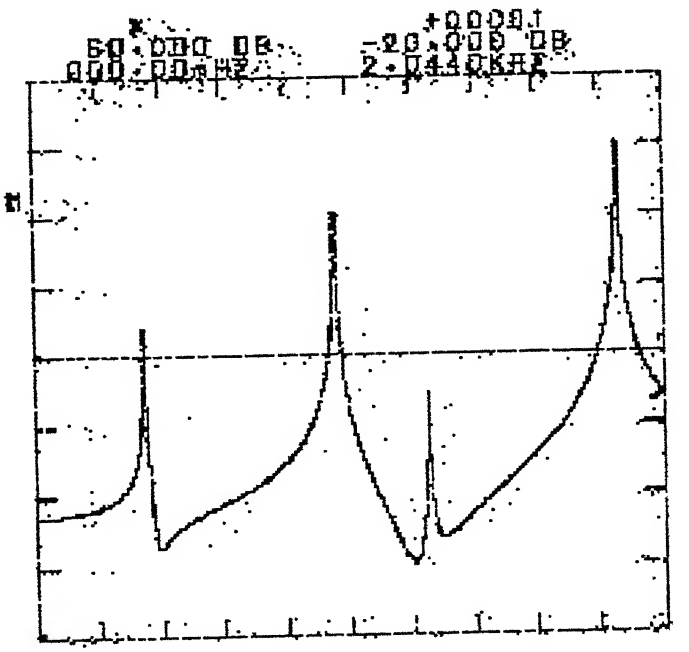

Fig.4.13(b): $|\bar{a}^{a}_{\theta_2\theta_2}|$

Fig. 4.13 : Rotational FRFs calculated from regenerated substructure FRFs

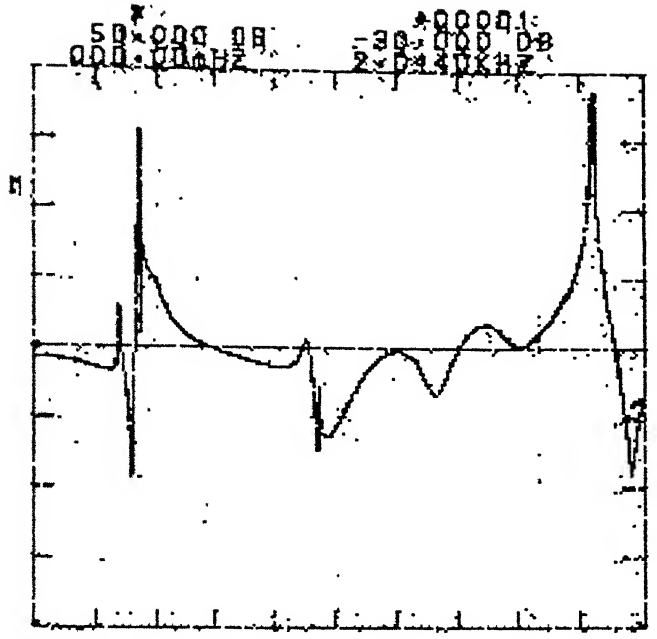

Fig.4.14(a): $|\bar{a}^{c}_{y_3\theta_3}|$

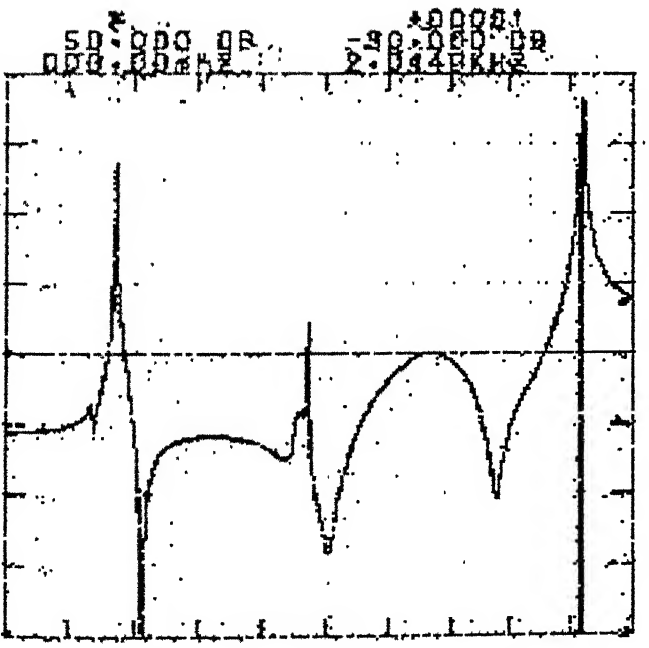

Fig.4.14(b) : $|\bar{a}^{c}_{\theta_1\theta_3}|$

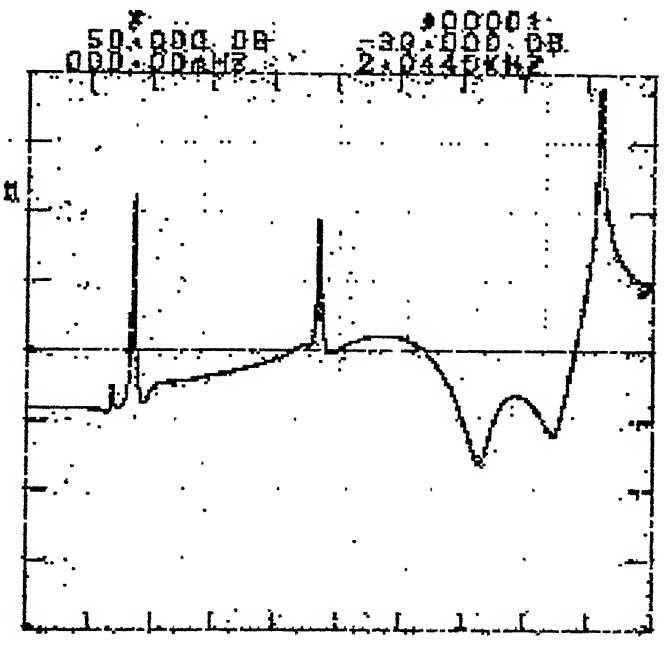

Fig. 4.14 (c): $|\bar{a}^{c}_{\theta_3\theta_3}|$

Fig.4.14 : Two-point Two-dof coupling: Predicted responses of coupled structure.

CHAPTER 5

GENERAL DISCUSSION

The original aim of this work was to predict the response of an assembly of identical simple beams when

i) The receptance properties of the simple beam is experimentally available, and

ii) The out of plane bending oscillations are under study where the coupling between bending and torsional oscillations can take place due to unsymmetric configurations of coupled structures.

The simplest coupled structure was formed with two identical beams with included angle equal to 180°. The bending and torsional modes are uncoupled in this configuration. The attempt to predict the response of this coupled structure failed since the predicted response exhibited peaks at all the natural frequencies of the substructure simple beam. Inclusion of more number of modes in the receptance data did not improve the results. Then two point coupling with two degrees of freedom associated with each point was tried. This improved the results marginally. Lack of time prevented trying out more number of coupling points. The experimental data then becomes so large that it is really not very practical to use this method of prediction.

Figures 4.12 and Figs. 3.9 are reproduced here in Fig. 5.1 to observe that the experimental FRFs match quite well with the theoretical FRF (using Appendix D). As evident from the theoretical results in Figs. 3.10, the impedance coupling method employed is perfectly correct. Then the anomaly could only result from the fact that the nature of impedance coupling is such that a small inaccuracy in the receptances of substructure causes inaccurate results.

In order to narrow down the source of error, a trial was made with coupling of two nonidentical beams. The beams were similar in all dimensions and properties except that the length of one beam was increased to 0.42 m. Fig. 5.2(a) shows the two substructures and the points considered for coupling. The "one point two degree of freedom coupling" (Section 3.3.4) was applied, the coupling point being the point number 1. Fig. 5.2(b) shows the regenerated accelerances $\bar{a}^{a}_{y_1y_1}$ and $\bar{a}^{b}_{y_1y_1}$. The predicted accelerance for coupled structure is shown in Fig. 5.2(c) which also includes the accelerance obtained experimentally for the coupled structure. The predicted response is still not good but it is evident that the peaks in predicted response do not always correspond to the substructure natural frequencies. It is felt that if the difference in lengths of the two beams was larger, the predicted response would appear closer to the expected response.

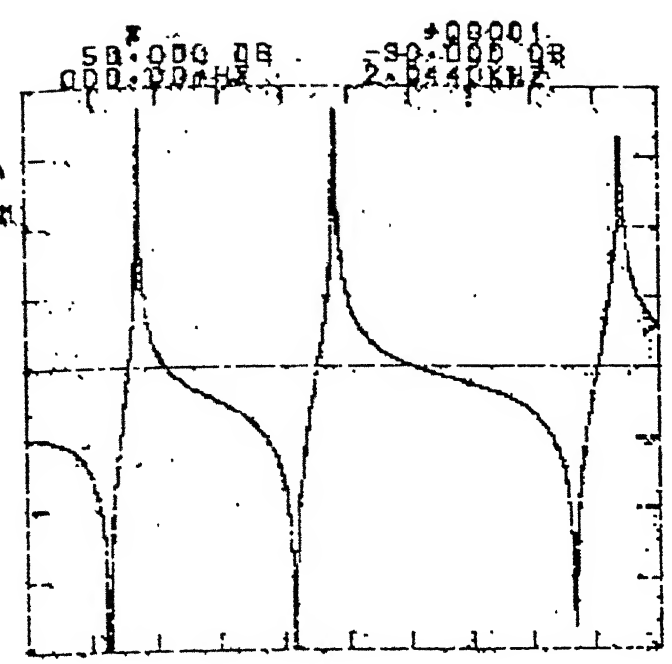

$|\bar{a}^{a}_{y_2y_2}|$

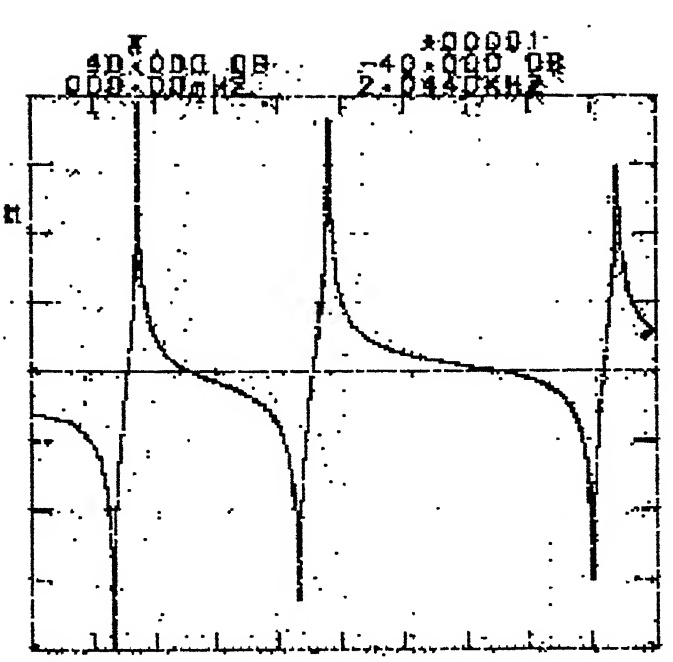

$|\bar{a}^{a}_{y_1y_2}|$

Theoretical

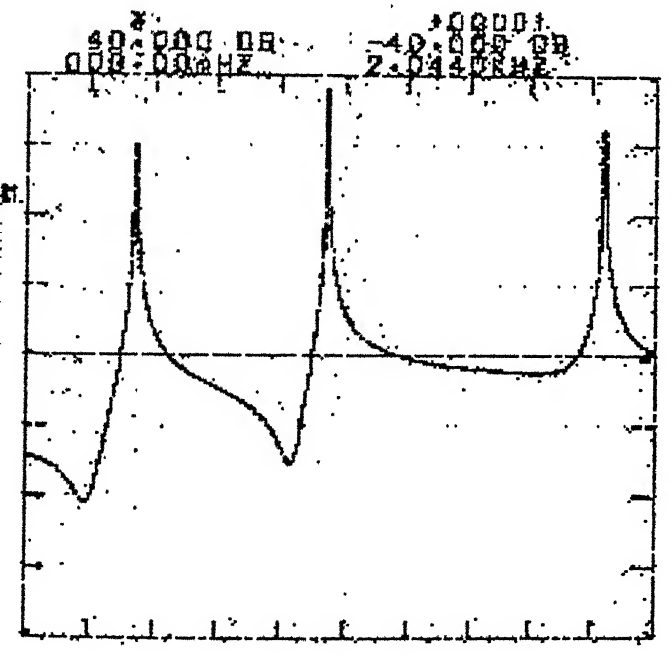

$|\bar{a}^{a}_{y_2y_2}|$

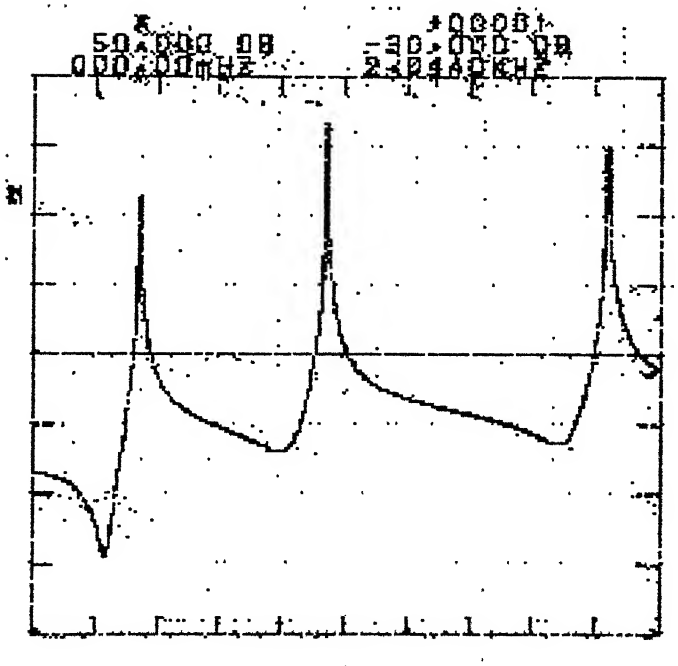

$|\bar{a}^{a}_{y_1y_2}|$

Experimental

Fig.5.1 : Theoretical and experimental FRFs for comparison

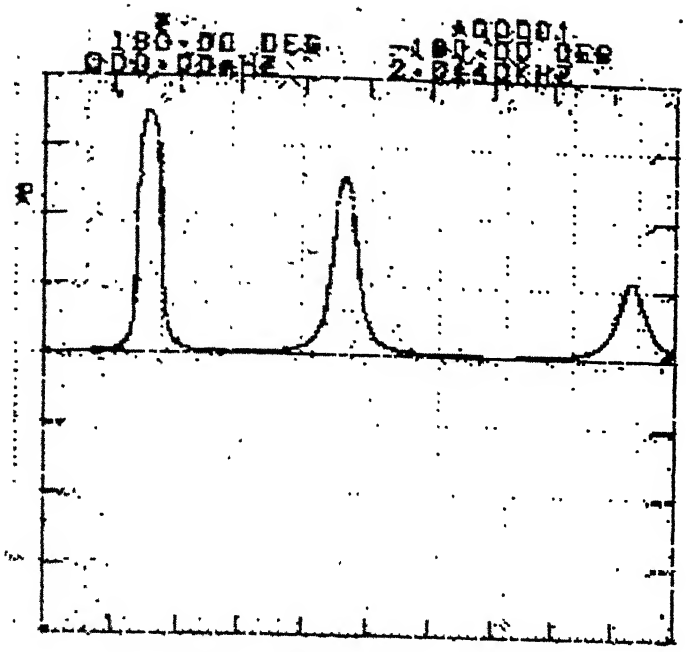

$\bar{a}^{a}_{y_2y_2}$

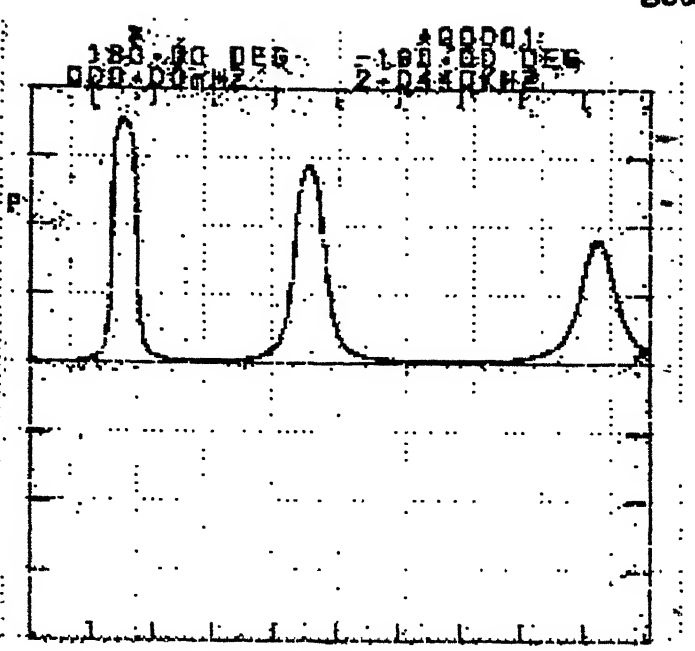

$\bar{a}^{a}_{y_1y_2}$

Theoretical

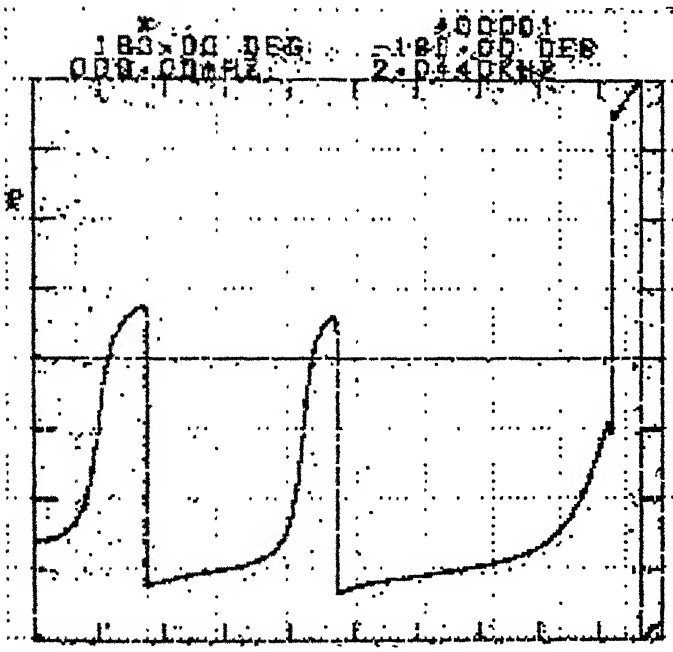

$\bar{a}^{a}_{y_2y_2}$

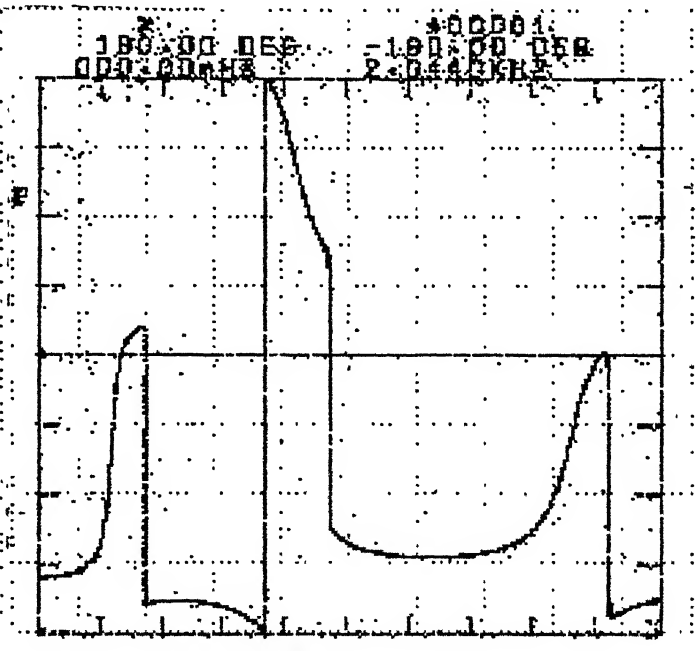

$\bar{a}^{a}_{y_1y_2}$

Experimental

Fig. 5.1(b) : Theoretical and Experimental Phase Plots for Comparison

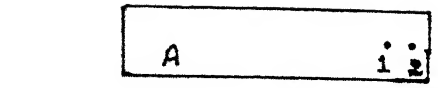

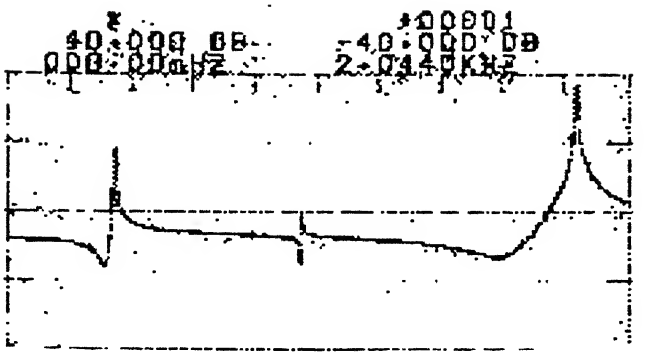

$|\bar{a}^{a}_{y_1y_1}|$

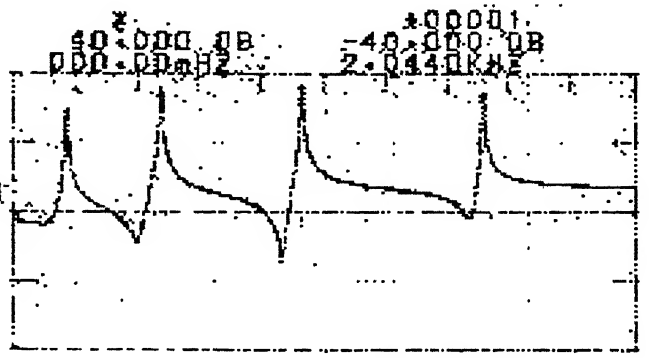

$|\bar{a}^{b}_{y_1y_1}|$

Fig.5.2(a)

Fig. 5.2(b)

Fig.5.2(b) : Regenerated substructure FRFs of beam A(l = 0.3m) and beam B (l = 0.42 m)

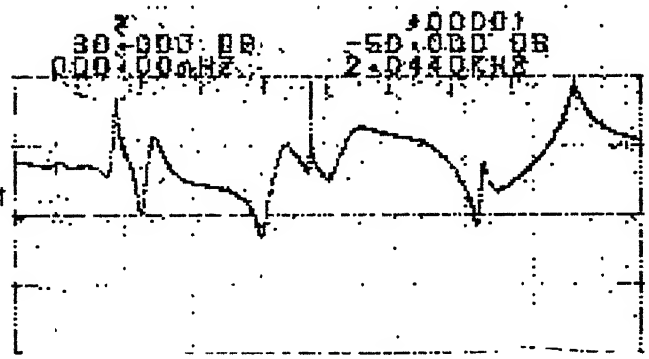

Predicted $|\bar{a}^{c}_{y_1y_1}|$

Fig.5.2(c): One-point Two-dof coupling: Predicted and measured coupled structure FRF.

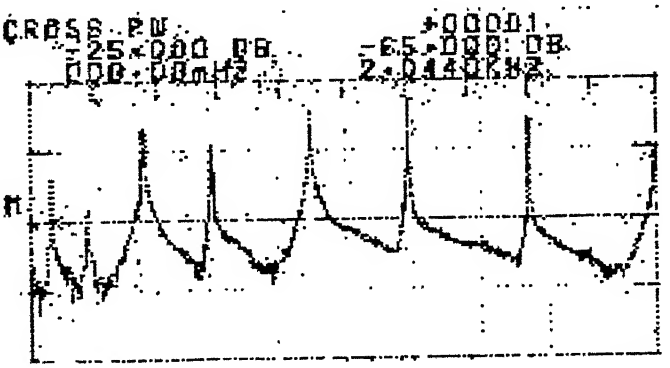

Measured $|\bar{a}^{c}_{y_1y_1}|$

Fig. 5.2(c)

An error analysis of the impedance coupling of two identical beams is expected to reveal the exact source of error in predicting the response of coupled structure.

REFERENCES

1. Jaspal Singh, "Some Investigations of Modal Analysis Technique", M.Tech. Thesis, IIT Kanpur, July 1988.

2. Vasudeva Rao, B.V., "Experimental Verification of Some Modal Analysis Methods", M.Tech. Thesis, IIT Kanpur, October, 1988.

3. Ewins, D.J., "Modal Testing :"Theory and Practice", Research Studies Press Ltd., 1986.

4. Grief, R., "Substructuring and Component Mode Synthesis", The Shock and Vibration Digest, 18(7), 3-8, 1986.

5. Smith, J.E., "Measurement of the Total Structural Mobility Matrix", Shock & Vibration Bulletin, 40, 1970.

6. Ewins, D.J. and Sainsbury, M.G., "Mobility Measurement for the Vibration Analysis of Connected Structures". Shock and Vibration Bulletin, 42, 105-122, 1972.

7. Sattinger, S.S., "A Method for Experimentally Determining Rotational Mobilities of Structures", Shock and Vibration Bulletin, 50, 17-28, 1980.

8. Chen. W.H. and Cherng, J.S., "Modal Synthesis via Combined Experimental and Finite Element Techniques with Consideration of Rotational Effects", Journal of Sound and Vibration, 103(1), 1-11, 1985.

9. Ewins, D.J., Silva. J.M.M., and Maleci, G., "Vibration Analysis of a Helicopter with an Externally - Attached Carrier Structure". Shock and Vibration Bulletin, 50, Part 2, 155-171, September 1980.

10. Goyder, H.G.D., "Methods and Application of Structural Modelling from Measured Structural Frequency Response Data", Journal of Sound and Vibration, 68(2), 209-230, 1980.

11. Natke, H.G., "Modal Synthesis - Modal Correction-Modal Coupling", Identification of Vibrating Structures, Springer Verlag Wien - New York, 1982.

12. Lee. J.M., "A Study of the Dynamical Modelling of Structures with Bolted and Bearing Joints", Annals of CIRP, 37(1), 343-346, 1988.

13. Schwartz, H.Z., "Numerical Techniques in Finite Element Method", 185-201, 1988.

14. Craig, R.R., "Structural Dynamics", John Wiley and Sons, 467-495, 1981.

15. Bishop, R.E.D. and Johnson, D.C., "The Mechanics of Vibration", Cambridge University Press, 1960.

16. Blevins, R.D., "Formulas for Natural Frequency and Mode Shape", Van Nostrand Reinhold Company, 1979.

17. Chhang. C.H., "Vibrations of Frames with Inclined Member Journal of Sound and Vibration, 56(2), 201-214, 1978.

18. Snowdon, J.C., "Vibration and Shock in Damped Mechanical Systems", John Wiley Sons, Inc., 1968.

APPENDIX A

GEOMETRIC AND MATERIAL PROPERTIES OF BEAM ELEMENTS

Beams considered are of mild steel material. These have the following properties:

E = Young's modulus = 2.1×10^{11} N/m^2

ν = Poisson's ratio = 0.3

G = Shear modulus = $\frac{E}{2(1+\nu)}$ = 8.1×10^{10} N/m^2

ρ = Mass density = 7.8×10^{3} kg/m^3

a = Width of beam = 0.05 m

b = Thickness of beam = 0.006 m

l = Length of the beam = 0.3 m, 0.42 m depending on the case

A = Area of cross section = 3×10^{4} m^2

I = Area moment of inertia = $\frac{ab^3}{12}$ = 9×10^{-10} m^4

I_p = Polar moment of inertia = $\frac{ab^3}{12} + \frac{a^3b}{12}$

C = Torsion constant = $\frac{k.a^3b^3}{(a^2+b^2)}$

where, k for rectangular cross section depends on the a/b ratio [16

for a/b = 8, k = 0.312.

In the present case $a/b \simeq 8$

$\Rightarrow \quad C = 3.32 \times 10^{-9}$

APPENDIX B

FREQUENCY RESPONSE FUNCTIONS (FRFs)

Frequency response function (transfer function) is the ratio of output of a system to its input. Depending upon the output selected, the FRFs are classified into three groups as explained below.

(i) Accelerance $[\bar{a}(\omega)]$: Accelerance is the ratio of acceleration to the force of excitation.

$$\bar{a}(\omega) = \frac{\text{acceleration } (\ddot{x})}{\text{force } (f)}$$

(ii) Mobility $[Y(\omega)]$: Mobility is the ratio of velocity to force of excitation

$$Y(\omega) = \frac{\text{Velocity } (\dot{x})}{\text{force } (f)}$$

(iii) Receptance $[\alpha(\omega)]$: Receptance is the ratio of displacement to force of excitation

$$[\alpha(\omega)] = \frac{\text{displacement}(x)}{\text{force}}$$

For harmonic vibration, the relationship among the above mentioned FRFs is given below:

$$A(\omega) = \frac{\ddot{x}}{f} = -\omega^2 \alpha(\omega)$$

$$Y(\omega) = \frac{\dot{x}}{f} = i\omega \alpha(\omega)$$

For a beam, the responses x_1 and x_2 at two points 1 and 2 in terms of receptances can be obtained as

$$x_1 = \alpha_{11} f_1 + \alpha_{12} f_2$$

$$x_2 = \alpha_{12} f_1 + \alpha_{22} f_2$$

This can be written in matrix form as,

$$\{x_i\} = [\alpha] \{f_i\}$$

where

$$x_i = \{x_1 \quad x_2\}^T$$

$$f_i = \{f_1 \quad f_2\}^T$$

$$[\alpha] = \begin{bmatrix} \alpha_{11} & \alpha_{12} \\ \alpha_{12} & \alpha_{22} \end{bmatrix}$$

The various terminology used with the FRFs is explained below:

A point receptance is one where the response coordinate and the excitation coordinate are identical. A transfer receptance is one where the response and excitation coordinates are different.

These are further subdivided into direct and cross-receptances. Direct receptance is one where the type of coordinates for response and excitation are identical - for example, both in y-direction. Cross receptance is one where the type of coordinates for response and excitation are not identical like one is y-direction translation and other is a moment in the z-direction. Following are some typical examples:

(i) Direct point receptances,

$$\alpha_{y_i y_i} = \frac{\text{Response in y-direction at i}}{\text{Force in y-direction at point i}},$$

$$\alpha_{\theta_i \theta_i} = \frac{\text{Rotation about z-axis at point i}}{\text{Moment about z-axis at point i}}$$

(ii) Cross point receptances,

$$\alpha_{y_I \theta_i} = \frac{\text{Translation in y-direction at point i}}{\text{Moment about x or z-direction at point i}}$$

(iii) Direct transfer receptance,

$$\alpha_{y_i y_j} = \frac{\text{Translation in y-direction at point i}}{\text{Force in y-direction at point j}}$$

(iv) Cross transfer receptance,

$$\alpha_{y_i \theta_j} = \frac{\text{Translation in y-direction at point i}}{\text{Moment in x or z-direction at point j}}$$

$$\lambda^4 = \frac{\omega^2 A \rho}{EI}$$

A = Area of cross section, m^2

ρ = Mass density, kg/m^3

ω = Frequency in rad/sec

$F_1 = \sin\lambda\ell \quad \sinh\lambda\ell$

$F_3 = (\cos\lambda\ell \quad \cosh\lambda\ell)^{-1}$

$F_5 = \cos\lambda\ell \quad \sinh\lambda\ell - \sin\lambda\ell \quad \cosh\lambda\ell$

$F_6 = \cos\lambda\ell \sinh\lambda\ell + \sin\lambda\ell \quad \cosh\lambda\ell$.

The receptance matrix for the coupled structure is given by

$$[\alpha^c(\omega)] = [[(\alpha^a(\omega)]^{-1} + [\alpha^b(\omega)]^{-1}]^{-1}$$

or,

$$[\alpha^c(\omega)]_{y_1,\theta_1} = \frac{(F_5 F_6 + F_1^2)}{2F_5F_6 \cdot EI\lambda \cdot F_3} \begin{bmatrix} -F_5/\lambda^2 & 0 \\ 0 & F_6 \end{bmatrix}$$

For the maximum value of $\alpha^c_{y_1y_1}$ or $\alpha^c_{\theta_1\theta_1}$, the denominator of the factor $\frac{F_5F_6 + F_1^2}{2F_5F_6.EI\lambda.F_3}$ should be minimum. Substituting for F_1, F_3, F_5 and F_6 and simplifying,

$$\frac{(F_5 F_6 + F_1^2)}{2F_5 F_6 \cdot EI\lambda \cdot F_3} = \frac{(\cos\lambda\ell.\cosh\lambda\ell + 1)}{EI\lambda.(\cos 2\lambda\ell.\cosh 2\lambda\ell - 1)}$$

APPENDIX D

ONE POINT 2 DOF COUPLING USING THEORETICAL RECEPTANCES FOR A DAMPED STRUCTURE

The point receptance at point '0' and the transfer receptance points p and 0 as given by [18] are,

$$\alpha_{oo} = \frac{(1+\mu)\,(n^* a)\,\varepsilon^*}{-\omega^2 \cdot 2\sigma^* M_b}$$

$$\alpha_{op} = \frac{(1+\mu)\,(n^* a)\,\Omega_\lambda^*}{-\omega^2\, 4\,\sigma^* M_b}$$

where,

ω - frequency of excitation

$$\sigma^* = [(Sh.C)(Sh.C)_\mu + (Ch.C)(Ch.C)_\mu - (Sh.S)(Sh.S)_\mu - (Ch.S)(Ch.S)_\mu - 1]_{(n^* a)}$$

$$\varepsilon^* = [(Ch.C+1)(Sh.C-Ch.S)_\mu + (Ch.C+1)_\mu (Sh.C-Ch.S)]_{(n^* a)}$$

$$\Omega_\lambda^* = [(\varepsilon^*+\beta^*) \operatorname{Cosh} n^*\lambda a + (\varepsilon^* - \beta^*) \operatorname{Cos} n^*\lambda a - (\sigma^* + \kappa^* + \chi^*) \operatorname{Sinh} n^*\lambda a + (\sigma^* - \kappa^* + \chi^*) \operatorname{Sin} n^*\lambda a]$$

in which,

$$\delta_e = 0.003$$

The notation $[(Sh.C - Ch.S)_{\mu}]_{(n^*a)}$ means

$[Sinh\ (\mu n^* a) \cdot Cos\ (\mu n^* a) - Cosh\ (\mu n^* a) \cdot Sin\ (\mu n^* a)]$.

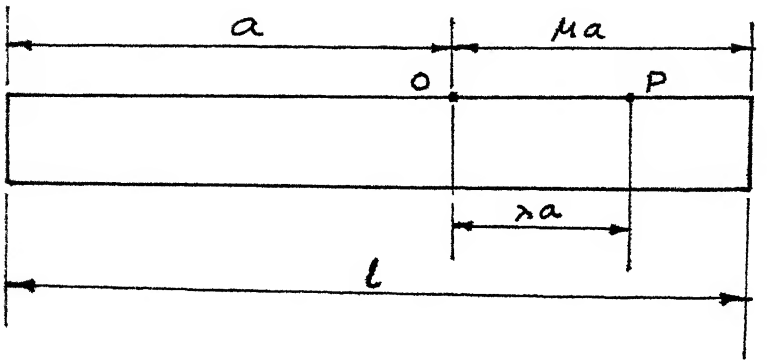

FIG. D.1

APPENDIX E

INVERSION OF A COMPLEX MATRIX

If the inverse of a complex matrix $[[A] + i\,[B]]$ is given by $[[C] + i[D]]$, then,

$$([A] + i[B])\,([C] + i\,[D]) = [1] + i\,[0]$$

$$([A]\,[C] - [B]\,[D]) + i\,([B]\,[C] + [A][D]) = [1] + i[0] \tag{E.1}$$

From (E.1)

$$[A]\,[C] - [B]\,[D] = [1] \tag{E.2}$$

$$[B]\,[C] + [A]\,[D] = [0] \tag{E.3}$$

Solving (E.2) and (E.3) for [C] and [D] we get,

$$[C] = ([A] + [B]\,[A]^{-1}\,[B])^{-1},$$

$$[D] = -[A]^{-1}\,[B]\,([A] + [B]\,[A]^{-1}\,[B])^{-1}.$$

The real matrix inversion required above, was done using usual inversion process by Gauss-Jordan's method.

APPENDIX F

Elements of Matrix [M]:

$M(1,1) = M(1,3) = 0$

$M(1,2) = -E_1 I_1 K_{1b}^2$

$M(1,4) = E_1 I_1 K_{1b}^2$

$M(1,5) = M(1,6) = M(1,7) = M(1,8) = M(1,9) = M(1,10) = M(1,11) =$

$M(2,1) = - E_1 I_1 K_{1b}^3$

$M(2,2) = 0$

$M(2,3) = E_1 I_1 K_{1b}^3$

$M(2,4) = M(2,5) = M(2,6) = M(2,7) = M(2,8) = M(2,9) = M(2,10) = M(2,11) = 0$

$M(3,1) = -E_1 I_1 K_{1b}^3 \text{Cos} K_{1b} l_1$

$M(3,2) = E_1 I_1 K_{1b}^3 \text{Sin} K_{1b} l_1$

$M(3,3) = E_1 I_1 K_{1b}^3 \text{Cosh} K_{1b} l_1$

$M(3,4) = E_1 I_1 \text{Sinh} K_{1b} l_1$

$M(3,5) = E_2 I_2 K_{2b}^3$

$M(3,6) = 0$

$M(3,7) = -E_2 I_2 K_{2b}^3$

$M(3,8) = M(3,9) = M(3,10) = M(3,11) = 0$

$M(4,1) = -E_1 I_1 K_{1b}^2 \text{Sin} K_{1b} l_1$

$M(4,2) = -E_1 I_1 K_{1b}^2 \text{Cos} K_{1b} l_1$

$M(4,3) = E_1 I_1 K_{1b}^2 \text{Sinh} K_{1b} l_1$

$M(4,4) = E_1 I_1 K_{1b}^2 \text{Cosh} K_{1b} l_1$

$M(4,5) = 0$

$M(4,6) = -E_2 I_2 K_{2b}^2 \cos 2\Gamma$

$M(4,7) = 0$

$M(4,8) = E_2 I_2 K_{2b}^2 \cos 2\Gamma$

$M(4,9) = 0$

$M(4,10) = -G_2 C_2 K_{2\theta} \sin 2\Gamma$

$M(4,11) = 0$

$M(5,1) = M(5,2) = M(5,3) = M(5,4) = M(5,5) = M(6,7) = M(5,11) =$ (

$M(5,6) = -E_2 I_2 K_{2b}^2 \sin 2\Gamma$

$M(5,8) = E_2 I_2 K_{2b}^2 \sin 2\Gamma$

$M(5,9) = -G_1 C_1 K_{1\theta} \sin K_{1\theta} l_1$

$M(5,10) = G_2 C_2 K_{2\theta} \cos 2\Gamma$

$M(6,1) = M(6,2) = M(6,3) = M(6,4) = M(6,9) = M(6,10) = M(6,11) =$

$M(6,5) = -E_2 I_2 K_{2b}^2 \sin K_{2b} l_2$

$M(6,6) = -E_2 I_2 K_{2b}^2 \cos K_{2b} l_2$

$M(6,7) = E_2 I_2 K_{2b}^2 \sinh K_{2b} l_2$

$M(6,8) = E_2 I_2 K_{2b}^2 \cosh K_{2b} l_2$

$M(7,1) = M(7,2) = M(\&,3) = M(7,4) = M(7,9) = M(7,10) = M(7.11) =$

$M(7,5) = -E_2 I_2 K_{2b}^3 \cos K_{2b} l_2$

$M(7,6) = E_2 I_2 K_{2b}^3 \sin K_{2b} l_2$

$M(7,7) = E_2 I_2 K_{2b} \cosh K_{2b} l_2$

$M(7,8) = E_2 I_2 K_{2b}^3 \sinh K_{2b} l_2$

$M(8,1) = M(8,1) = M(8,3) = M(8,4) = M(8,5) = M(8,6) = M(8,7)$
$= M(8,8) = M(8,9) = 0$

$M(8,10) = G_2 C_2 K_{2\theta} \text{Cos } K_{2\theta} l_2$

$M(8,11) = -G_2 C_2 K_{2\theta} \text{Sin } K_{2\theta} l_2$

$M(9,1) = \text{Sin } K_{1b} l_1$

$M(9,2) = \text{Cos } K_{1b} l_1$

$M(9,3) = \text{Sinh } K_{1b} l_1$

$M(9,4) = \text{Cosh } K_{1b} l_1$

$M(9,5) = M(9,7) = M(9,9) = M(9,10) = M(9,11) = 0$

$M(9,6) = -1$

$M(9,8) = -1$

$M(10,1) = K_{1b} \text{Cos } K_{1b} l_1$

$M(10,2) = -K_{1b} \text{Sin } K_{1b} l_1$

$M(10,3) = K_{1b} \text{Cosh } K_{1b} l_1$

$M(10,4) = K_{1b} \text{Sinh } K_{1b} l_1$

$M(10,5) = K_{2b} \text{Cos2r}$

$M(10,6) = M(10,8) = M(10,9) = M(10,10) = 0$

$M(10,7) = K_{2b} \text{Cos } 2r$

$M(11,1) = M(11,2) = M(11,3) = M(11,4) = M(11,6) = M(11,8)$
$= M(11,10) = 0$

$M(11,5) = K_{2b} \text{Sin2r}$

$M(11,7) = K_{2b} \text{Sin2r}$

$M(11,9) = \text{Cos } K_{1\theta} l_1$

$M(11,11) = \text{Cos2r}$

ME-1989-M-VIS-DIFF